JGR Atmospheres

RESEARCH ARTICLE
10.1029/2022JD037660

Global and Regional Characteristics of Radially Outward Propagating Tropical Cyclone Diurnal Pulses

Xinyan Zhang[1,2], Sarah D. Ditchek[3,4], Kristen L. Corbosiero[5], and Weixin Xu[1,2]

[1]Southern Marine Science and Engineering Guangdong Laboratory (Zhuhai) & School of Atmospheric Sciences, Sun Yat-Sen University, Zhuhai, China, [2]Guangdong Province Key Laboratory for Climate Change and Natural Disaster Studies, Guangzhou, China, [3]Cooperative Institute for Marine and Atmospheric Studies, University of Miami, Miami, FL, USA, [4]NOAA/OAR/Atlantic Oceanographic and Meteorological Laboratory, Miami, FL, USA, [5]Department of Atmospheric and Environmental Sciences, University at Albany, State University of New York, New York, NY, USA

Abstract The radially outward propagating, cloud top cooling, diurnal pulse (DP) is a prominent feature in tropical cyclones (TCs) that has important implications for changes in TC structure and intensity. By using an objective identification algorithm, this study characterizes DPs over various ocean basins and examines their environmental conditions and convective structures. DPs occur on 52% of TC days globally and the occurrence frequency exhibits significant regional variability. The Northwest Pacific (NWP) has the highest DP frequency (60%) and shares the largest fraction of DPs worldwide (34%). The median duration and propagation distance of DPs are 12–15 hr and 500–600 km, respectively. Although the mean propagation speed of DPs is 11–13 m s^{-1}, persistent DPs (lasting >15 hr) mostly propagate at speeds similar to internal inertial gravity waves (5–10 m s^{-1}). Additionally, the longer the pulse duration, the stronger the pulse amplitude. Further, most DPs initiate in the inner core overnight, in phase with inner-core deep convection. Inner-core cold clouds, precipitation, and lightning are all markedly enhanced on DP days compared to non-DP days. Interestingly, the DP signal significantly weakens and becomes slower while propagating through the 200–400-km annulus during 09–12 local time (LT). Finally, DPs are more likely to occur over warm sea surface temperatures (SSTs), in low shear, and with a moist mid-to-upper troposphere. SST plays an important role in DP development over all basins, while shear and humidity are less important in the Northeast Pacific (NEP) and North Atlantic (NA) basins.

Plain Language Summary One of the most prominent diurnal features in tropical cyclones (TCs) is the radially outward propagation of a cooling signal in the upper-level clouds, the so-called diurnal pulse. Diurnal pulses occur not only at the cirrus canopy but also in the deep convective layer, possibly imposing a significant impact on the internal structures and intensity change of TCs. Therefore, it is necessary to investigate properties of TC diurnal pulses in depth. This study identifies thousands of TC diurnal pulse events worldwide from 2001 to 2018 using long-term satellite infrared brightness temperature data. Diurnal pulses occur on 52% of TC days globally. They are the most frequent over the Northwest Pacific. Both the global and regional properties of diurnal pulses are fully quantified, including the initial and ending time/location, duration, propagation length, propagation speed, and pulse amplitude. It is found that most diurnal pulses initiate in the inner core overnight with a median duration and propagation distance of 12–15 hr and 500–600 km, respectively. Environmental conditions and internal convective structures of TCs with and without diurnal pulses are further analyzed to investigate how the diurnal pulse impacts TC structure and what factors may influence the occurrence of diurnal pulses.

Key Points:

- Diurnal pulses occur on 52% of tropical cyclone (TC) days globally with significant regional variability, and most of them follow the diurnal clock
- The median duration (propagation distance) of diurnal pulses is 12–15 hr (500–600 km) and long-lived pulses travel at 5–10 m s^{-1}
- Diurnal pulses are more likely to occur in TCs with strong inner-core convection and environments favorable for TC intensification

Supporting Information:

Supporting Information may be found in the online version of this article.

Correspondence to:

W. Xu,
xuwx25@mail.sysu.edu.cn

Citation:

Zhang, X., Ditchek, S. D., Corbosiero, K. L., & Xu, W. (2023). Global and regional characteristics of radially outward propagating tropical cyclone diurnal pulses. *Journal of Geophysical Research: Atmospheres*, *128*, e2022JD037660. https://doi.org/10.1029/2022JD037660

Received 12 AUG 2022
Accepted 10 MAR 2023

1. Introduction

Tropical cyclones (TCs) are one of the most catastrophic natural hazards, causing thousands of deaths and billions of dollars in economic losses every year (Emanuel et al., 2012; Mori & Takemi, 2016; Weinkle et al., 2012; Zhang et al., 2009, 2017). Over the last few decades, TC intensity change has been extensively researched, and significant progress to our understanding has been achieved (Demaria et al., 2014; Leroux et al., 2018; Rogers, 2021; Wang, 2014, 2018; Wang & Wu, 2004). However, forecasting TC intensity change, especially rapid intensification, still faces great challenges (Demaria et al., 2014; Leroux et al., 2018), as intensity change is impacted by complex processes across multiple scales involving both environmental forcing and internal structures (Hendricks et al., 2010; Kaplan & Demaria, 2003; Rogers, 2021; Wang & Wu, 2004). The diurnal cycle of

TCs is likely one such process (Melhauser & Zhang, 2014; Ruppert & Hohenegger, 2018; Tang & Zhang, 2016). For example, recent observational studies have shown that the diurnal cycle of TC convection is closely related to TC intensity change (Lee et al., 2020; Sun et al., 2021; Wu et al., 2020; Zhang & Xu, 2021b).

TCs show significant diurnal variations in many aspects related to TC convection that could impact TC intensity (e.g., Dunion et al., 2014; Kossin, 2002; Lee et al., 2020; Leppert & Cecil, 2016; Zhang et al., 2020; Zhang & Xu, 2021a, 2022). Instability, relative humidity, and low-level inflow are all enhanced at night, likely due to the nocturnal radiation-convection interaction and differential radiative cooling between convective and clear-sky areas (Duran et al., 2021; Ruppert & Hohenegger, 2018; Zhang et al., 2020). This interaction could invigorate precipitation, deep convection, and lightning activity around midnight and into the early morning hours (Leppert & Cecil, 2016; Sun et al., 2021; Tang et al., 2019; Zhang & Xu, 2021a). Conversely, daytime convection is suppressed because of increased stability and boundary layer downdrafts produced by nighttime deep convection (Bowman & Fowler, 2015; Zhang et al., 2020; Zhang & Xu, 2021a). The upper-level outflow and cirrus canopy areal extent both maximize in the afternoon (Lee et al., 2020; Muramatsu, 1983; Ruppert & O'Neill, 2019; Wu & Ruan, 2016), leading to a time offset (~12 hr) between the diurnal cycles of the surface precipitation and cloud anvil (Dunion et al., 2014; Kossin, 2002; Wu & Ruan, 2016). Model simulations suggest that the upper-level outflow and cirrus canopy are likely lifted and enhanced in response to shortwave radiative heating during daytime (Evans & Nolan, 2019; Ruppert & O'Neill, 2019). A schematic of the timing of these processes was summarized by Ditchek, Corbosiero, et al. (2019) and Ditchek, Molinari et al. (2019, their Figure 1).

Another diurnal variation found in TCs that could impact TC intensity is a cloud top cooling signal (the so-called "diurnal pulse," hereafter DP) that propagates radially outward over the course of the day (Ditchek, Corbosiero, et al., 2019; Ditchek, Molinari, et al., 2019; Ditchek et al., 2020; Duran et al., 2021; Kossin, 2002). The pulse is identified by taking 6-hr satellite infrared (IR) brightness temperature (BT) differences, and has been found to be related to the expansion and contraction of the cirrus canopy (Dunion et al., 2019; Melhauser & Zhang, 2014; Ruppert & O'Neill, 2019; Wu & Ruan, 2016). Initial studies on the DP focused on major hurricanes over the Atlantic Ocean (Dunion et al., 2014; Kossin, 2002). DPs were found to be a prominent feature of major hurricanes that propagated outward on a predictable schedule, so much so that Dunion et al. (2014) created a 24-hr conceptual clock to identify the location of the DP based on local time. Ditchek, Corbosiero, et al. (2019) generalized and expanded the work of Dunion et al. (2014) by using an objective metric to create a 1982–2017 climatology of DPs in Atlantic-basin TCs. They found that 45% of Atlantic-basin TCs produced DPs that lasted more than 9 hr, with 80% of major hurricane days having a DP. Ditchek, Corbosiero, et al. (2019) also found that some days without outward propagating diurnal "cooling pulses" had outward propagating warming cloud tops that followed the Dunion et al. (2014) conceptual clock. These diurnal "warming pulses" were also objectively identified and those that lasted more than 9 hr occurred 8.5% of the time.

While the DP has been identified using cloud top brightness temperature differences, it has also been found to impact the TC's deep-layer structure (Ditchek, Corbosiero, et al., 2019; Ditchek, Molinari, et al., 2019; Ditchek et al., 2020; Dunion et al., 2014, 2019; Duran et al., 2021). More than half of diurnal cooling pulses are coupled with surface precipitation and deep convection in TCs, including lightning and deep-layer ice water content (Ditchek, Molinari, et al., 2019; Zhang & Xu, 2022). DPs are also more likely to occur in stronger TCs over the open ocean, and TCs in environments with high sea surface temperatures (SSTs) and/or low vertical wind shear (Ditchek, Corbosiero, et al., 2019; Ditchek, Molinari, et al., 2019; Dunion et al., 2014, 2019), implying that a favorable environment for deep convection is beneficial for pulse propagation. In fact, at outer radii the pulses often have tropical squall-line characteristics (Ditchek et al., 2020; Dunion et al., 2019).

Numerical simulations suggest that the DP is possibly triggered by tropospheric internal inertial gravity waves due to inner-core deep convection (Evans & Nolan, 2019; Navarro & Hakim, 2016; Navarro et al., 2017; O'Neill et al., 2017; Ruppert & O'Neill, 2019). Conversely, Ditchek et al. (2020) performed a case study using observations and High-Resolution Rapid Refresh model output on DPs in Hurricane Harvey (2017) and found that a prominent DP was formed from reinvigorated inner rainbands that propagated outward into a more favorable environment for deep convection. Several other mechanisms have been proposed for the generation of DPs, including nighttime reduced outflow resistance (Mecikalski & Tripoli, 1998), differential heating between cloudy and cloud-free areas (Gray & Jacobson, 1977), direct radiation-convection interactions (Chen & Cotton, 1988; Kraus, 1963; Randall et al., 1991), and microphysical feedback processes between ice crystals and cloud water (Houze et al., 1981). The cause(s) of the pulse remains an area of active research.

Recent studies have found that the diurnal cycle of convection and the DP are closely related to TC intensity change (Lee et al., 2020; Sun et al., 2021; Wu et al., 2020; Wu & Hong, 2022; Zhang & Xu, 2021b). Rapidly intensifying TCs often experience more pronounced diurnal variations in many aspects of TC structure, including stronger nighttime enhancement of TC cold clouds (Wu et al., 2020) and deep convective bursts (Sun et al., 2021), as well as eyewall and radius of maximum wind contraction (Lee et al., 2020; Wu & Hong, 2022), suggesting that nocturnally invigorated deep convection may contribute significantly to TC intensification. The frequency and duration of the DP were found to be well correlated to 24-hr TC intensification rate on the day before or during the occurrence of the pulse; for example, rapidly intensifying TCs have a higher likelihood to produce strong DPs (Zhang & Xu, 2021b). The DP has also been found to be associated with the rapid development of nighttime inner-core deep convection (Ditchek, Corbosiero, et al., 2019; Ditchek, Molinari, et al., 2019; Zhang & Xu, 2021b), which produces large amounts of latent heating in the inner core and stronger eye subsidence to enhance the warm core (Guimond et al., 2010; Rogers et al., 2016; Susca-Lopata et al., 2015; Vigh & Schubert, 2009). The outward propagation of the pulse may also strengthen and modify the TC radial-vertical circulation, leading to a positive feedback with TC intensification (Dunion et al., 2019; Muramatsu, 1983; O'Neill et al., 2017; Zhang et al., 2020).

Since the DP can impact both TC structure and intensity, it is necessary to investigate properties of DPs in depth. While DPs have been documented in the literature, they are mostly limited to those that occurred in Atlantic-basin TCs. To understand the overall and regional variability of DPs, this study investigates DPs in TCs worldwide from 2001 to 2018 when TC track records, satellite infrared (IR) data, satellite rainfall products, and most global lightning measurements are commonly available. By doing so, the following questions can be answered:

1. What are the overall characteristics (duration, propagation speed, propagation distance, initial time/location, etc.) of DPs in global TCs?
2. Do the frequency and properties of DPs exhibit significant regional variability and, if so, what are the underlying reasons?
3. What are the environmental factors and internal processes that affect the DP, and do they vary by region?
4. Do DPs influence the inner-core deep convection on the daily mean scale, for example, are there significant differences in the diurnal cycles of precipitation and intense convection (i.e., lightning) for TC days with and without a DP?

By answering these questions, this study will more thoroughly detail characteristics of TC DPs, their regional variability, and corresponding environmental factors and internal convective structures.

2. Data and Methods

2.1. TC Track and Intensity

Three-hourly TC track and 10-min averaged, maximum sustained 10-m wind speed (V_{msw}) data from 2001 to 2018 are retrieved from the version-4 International Best Track Archive for Climate Stewardship (IBTrACS, Knapp et al., 2010, 2018). Storm times included in this study satisfy that storm centers are within 35°S – 35°N and are located at least 100 km away from land. Additionally, subtropical and extratropical systems are excluded from this study. TCs are classified into four categories based on their V_{msw} as follows: (a) tropical depressions (TD; $V_{msw} < 34$ kt), (b) tropical storms (TS; 34 kt $\leq V_{msw} <$ 64 kt), (c) category 1–2 hurricanes (CAT1–2; 64 kt $\leq V_{msw} <$ 96 kt), and (d) category 3–5 hurricanes (CAT3–5; $V_{msw} \geq$ 96 kt). Global TCs are first examined overall and then separated into four major TC basins to assess regional variability: (a) the Northwest Pacific (NWP) basin (0° – 35°N; 105° – 180°E), (b) the Northeast Pacific (NEP) basin (0° – 35°N; 95° – 180°W), (c) the North Atlantic (NA) basin (0 – 35°N; 10 – 95°W), and (d) the South Indian Ocean (SI) basin (0° – 35°S; 35° – 125°E). Note that TCs in the South Pacific (SP) basin (0° – 35°S; 140°E – 110°W) and North Indian Ocean (NI) basin (0° – 25°N; 50° – 100°E) are excluded from regional-comparison analysis because the number of TC days in those basins are limited (Table 1, row 1).

2.2. Cloud Top IR, Precipitation, and Global Lightning

Cloud top IR brightness temperatures (BTs) were retrieved from the Gridded Satellite B1 (GridSat) data set of the National Oceanic and Atmospheric Administration (NOAA) Climate Data Record program (Knapp et al., 2011). GridSat provides multi-satellite merged, global IR, water vapor, and visible observations with a spatial resolution

Table 1
Number of TC Days and Number (Frequency) of DPs From 2001 to 2018 Globally and in Individual TC Basins for all TCs (ALL) and by TC Intensity

	Global	NWP	SI	NEP	NA	SP	NI
TC days							
	6,778	1,983	1,370	1,824	830	486	285
DPs (Frequency)							
ALL	3,518 (51.9%)	1,198 (60.4%)	695 (50.7%)	771 (42.3%)	446 (53.7%)	248 (51.0%)	160 (56.1%)
TD	614 (37.1%)	181 (45.4%)	122 (36.2%)	174 (28.7%)	46 (34.6%)	46 (50.0%)	45 (52.3%)
TS	1,330 (50.0%)	382 (57.4%)	307 (52.9%)	278 (41.3%)	194 (49.2%)	89 (43.8%)	80 (55.9%)
CAT 1–2	813 (60.7%)	303 (68.4%)	129 (53.1%)	181 (52.5%)	110 (65.5%)	63 (61.2%)	27 (71.0%)
CAT 3–5	761 (67.5%)	332 (69.7%)	137 (65.2%)	138 (69.0%)	96 (71.1%)	50 (56.8%)	8 (44.4%)

of 0.07° and a temporal resolution of 3 hr. This study uses the IR BT data in the 11-μm channel which has undergone inter-satellite calibration (Desormeaux et al., 1993; Knapp, 2008). The data retrieved for this study between 2001 and 2018 combines available observations from the Geostationary Operational Environmental Satellite (GOES), Meteosat (MET), FengYun (FY), and Himawari satellite systems covering the global range of 70°N–70°S (Knapp et al., 2011).

TC precipitation data during 2001–2018 is derived from the version 06 (final-run) Integrated MultisatellitE Rainfall from GPM (IMERG) product (Hou et al., 2014; Huffman et al., 2020). IMERG combines precipitation estimates from passive microwave (PMW) observations and PMW-calibrated IR data through a morphing algorithm (Joyce et al., 2004; Joyce & Xie, 2011), and is constrained by rain gauge data on a monthly scale. Compared with previous satellite precipitation products, IMERG has significant advantages in capturing the temporal and spatial variation of precipitation globally (Kim et al., 2017; Ma et al., 2021; Tan et al., 2019), although precipitation estimates near the coastline and complex terrain display larger uncertainties (Huffman et al., 2020; Kim et al., 2017). IMERG data provide instantaneous rain rate with a high spatiotemporal resolution of 0.5 hr and 0.1°. Only 3-hr IMERG precipitation records at the time of the best track (e.g., 00:00–00:30, 03:00–03:30, 06:00–06:30 UTC) are used to represent precipitation intensity.

Lightning flash locations in TCs are obtained from the World Wide Lightning Location Network (WWLLN; Abarca et al., 2010; Virts et al., 2013) over the 2005–2018 period. The lightning locations are interpolated onto storm center-relative grids with the same spatial resolution as GridSat (i.e., 0.07°). As the WWLLN provides continuous TC lightning data, lightning flashes within ±1.5 hr of the TC time are accumulated to derive a 3-hr lightning field to match the IMERG, IBTrACS, and GridSat resolutions. The detection efficiency of the WWLLN was relatively low in 2005 owing to a limited number of sensors but has grown continuously over time due to an increase in sensors and improvements to detection algorithms (Hutchins et al., 2012; Rodger et al., 2009). To account for this varying detection efficiency, adjustment factors were applied to the WWLLN data (DeMaria et al., 2012; Lin & Chou, 2020; Stevenson et al., 2016, 2018) so that the yearly WWLLN lightning density matches the lightning density climatology of measurements from the Lightning Imaging Sensor (LIS) onboard the Tropical Rainfall Measuring Mission (TRMM) and Optical Transient Detector (OTD; Cecil et al., 2014). The adjustment factors of the four TC-prone basins applied in this study are shown in Table S1 in Supporting Information S1, which are similar to the values for the NEP and NA basins from 2001 to 2014 found in Stevenson et al. (2018).

2.3. Environmental Conditions and Internal Convective Structures

The fifth generation of European Center for Medium-Range Weather Forecasts (ECMWF) reanalysis (ERA5) data (Hersbach et al., 2020) is used to calculate the environmental conditions surrounding TCs. ERA5 provides hourly estimates of climate variables on a 30-km grid from 1978 to the present. The variables analyzed in this study include SST, vertical wind shear (200–850 hPa), as well as lower-to-mid (700–925 hPa) and mid-to-upper (300–500 hPa) level relative humidity. These factors were chosen as they are important environmental factors that impact diurnal oscillations and TC intensity change (Ditchek, Corbosiero, et al., 2019; Ditchek, Molinari, et al., 2019; Knaff et al., 2019; Zhang et al., 2020).

Table 2
The Definitions of TC Internal-Structure Variables and Environmental Factors

Variables	Units	Definition
Intensity	kt	Maximum sustained 10-m surface wind speeds at the TC center
IR BT	K	Mean IR BT within the inner core (0–100 km)
IR BT 6-hr trend	K	Mean IR BT 6-hr trends within the inner core (0–100 km)
Cold-cloud coverage	%	Areal fraction of IR BT < 208 K within the inner core (0–100 km)
SST	°C	Mean SST between 0 and 500 km
Shear	m s^{-1}	Differences of the mean wind vectors within a 200–800 km annulus between 200 hPa and 850 hPa
RH mid-upper	%	Mean relative humidity within 200–800 km at 300–500 hPa
RH low-mid	%	Mean relative humidity within 200–800 km at 700–925 hPa

The internal-structure variables calculated in this study include the TC intensity, inner-core 6-hr IR BT trend, mean IR BT, areal coverage of very cold clouds (IR BT < 208 K), and rain rate as these variables are reported to be closely linked to the DP in previous studies (Ditchek, Corbosiero, et al., 2019; Ditchek, Molinari, et al., 2019; Wu et al., 2020; Zhang & Xu, 2021b, 2022). Definitions of internal-structure variables, as well as environmental factors, are provided in Table 2. All parameters are averaged over the period of 00–03 LT, prior to diurnal pulse initiation and propagation, to examine their potential influence(s) on days with and without DPs.

3. Diurnal Pulse Identification

A diurnal pulse initially referred to a cooling signature in the 6-hr IR BT difference field that radially propagates outward over the course of the day following the Dunion et al. (2014) diurnal clock schematic (Ditchek, Corbosiero, et al., 2019; Ditchek, Molinari, et al., 2019; Dunion et al., 2014, 2019; Zhang & Xu, 2021b, 2022). According to the Dunion et al. (2014) conceptual model, the DP initiates from the TC inner core in the early morning and propagates outward to several hundred kilometers by the end of the day. Using this diurnal pulse clock, Ditchek, Corbosiero, et al. (2019) developed an objective algorithm to extract DPs from the 6-hr IR BT difference fields of TCs over the Atlantic Ocean. The Ditchek, Corbosiero, et al. (2019) algorithm does an excellent job of identifying diurnal pulses with cooling signatures that follow the diurnal pulse clock; however, there were some pulses with cooling signatures that occurred outside of the pulse clock (Ditchek et al., 2020; Trabing & Bell, 2021). For example, the cloud top cooling signal may initiate in the afternoon or evening instead of the early morning and propagate further than the idealized maximum distance (600 km). Ditchek, Corbosiero, et al. (2019) also found diurnal pulses of the opposite sign (with warming signatures) during days without diurnal pulses with cooling signatures. They called these diurnal "warming" pulses and suggested that they might be associated with off-the-clock diurnal pulses with cooling signatures. This study considers these potential issues to more inclusively identify all TC cooling pulses.

Similar to Ditchek, Corbosiero, et al. (2019), the objective algorithm in this study calculates the IR BT 6-hr difference in TCs every 3-hr and identifies DPs based on the radial location of significant cloud top cooling signals. Different from Ditchek, Corbosiero, et al. (2019) and Ditchek, Molinari, et al. (2019), cooling signatures in this study do not have to follow the diurnal pulse clock proposed by Dunion et al. (2014). Rather, cooling signatures are only required to be continuous in time and space. The algorithm includes four main steps:

1. Calculate IR BT tendency fields: TC-centered IR BT fields are derived from GridSat within 800 km from the TC center. Since cold-cloud propagation may spread beyond 600 km from the TC center (e.g., Trabing & Bell, 2021), the range of the IR BT field is 200 km further than the extended version of the Dunion et al. (2014) diurnal clock applied in Ditchek, Corbosiero, et al. (2019). IR BT tendency fields are then created every 3 hr through the lifecycle of each TC by subtracting the current IR BT field from the field 6 hr earlier. Note that after restricting storm times to those where storm centers are >100 km from land (see Section 2.1), some data points are still situated over land; however, these points account for <10% of the area considered for both the inner (0–400 km) and outer radii (Table S2 in Supporting Information S1). Due to this relatively small sample, these points had insignificant impacts on the results (Figures S1–S3 in Supporting Information S1).

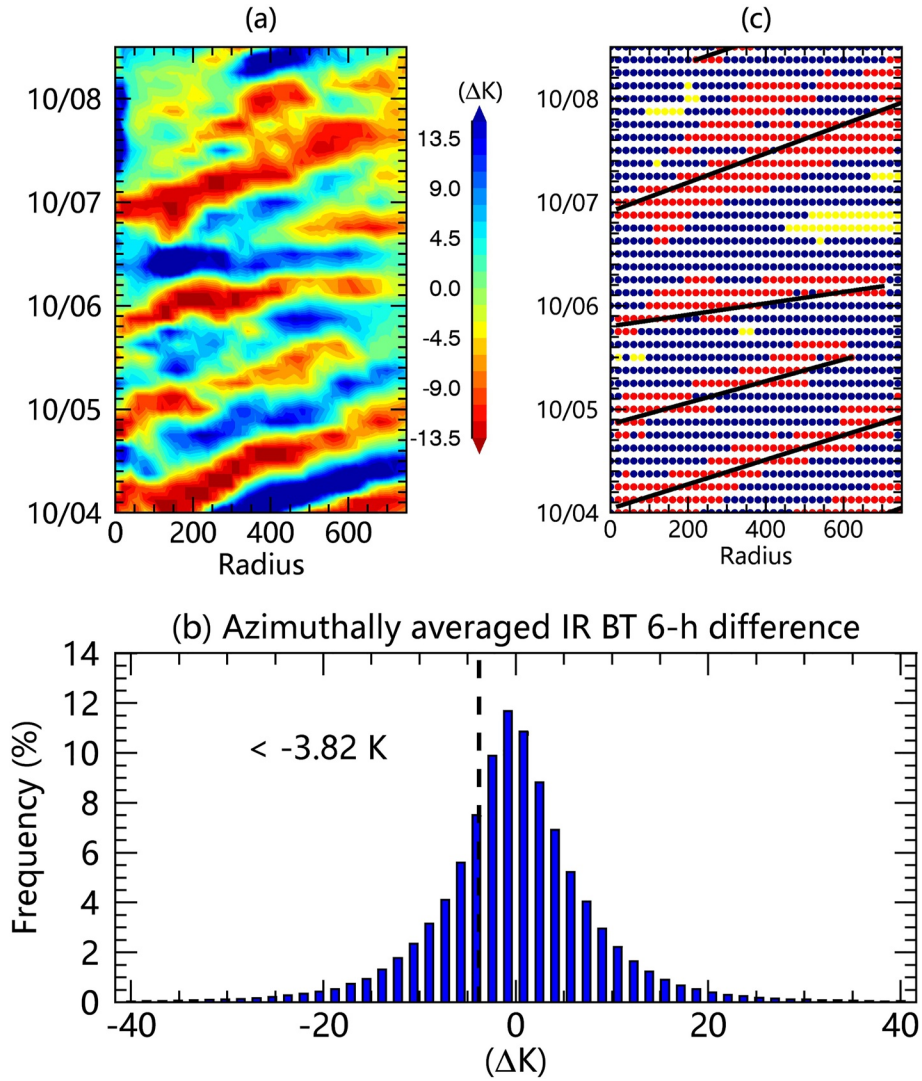

Figure 1. (a) Time-radius plot of azimuthally averaged IR BT trends of Super Typhoon Vongfong (2014) during 4–8 October; (b) probability distribution function (PDF) of azimuthally averaged IR BT 6-hr trends (current minus last 6 hr; K) in every 20-km annulus from 0to 800 km of all tropical cyclones (TCs), with the dashed line representing the threshold of significant cloud top cooling (lowest 25%, −3.82 K); (c) the propagation events classified from (a), where red dots represent grid points of significant cloud top cooling (<−3.82 k) within propagation events, yellow dots represent significant cloud top cooling grids without propagation events, and blue dots represent grid points that did not have significant cloud top cooling. Black lines are the fitted regression lines of the propagation events.

2. Compute TC lifecycle azimuthal-mean BT tendency: While Ditchek, Corbosiero, et al. (2019) found that only 6.8% of diurnal cooling pulses lasting more than 9 hr covered >50% of a radial ring, they still found a diurnal pulse signature when azimuthally averaging their 6-hr IR BT difference fields. This result was likely due to a smearing effect from pulses originating in different quadrants and propagating around each quadrant over their lifetime. Therefore, here the azimuthal mean of the IR BT tendency is calculated as a function of radial length and time (i.e., 20-km and 3-hr bins), yielding a time-radius distribution (i.e., Hovmöller diagram) of IR BT tendency for each individual storm throughout its life cycle. Figure 1a provides an example of the time-radius BT tendency distribution in Super Typhoon Vongfong during 4–8 October 2014.
3. Identify significant cloud top cooling grid points: The probability distribution function (PDF) of the azimuthally averaged IR BT tendency for the entire TC data set from 2001 to 2018 is then constructed (e.g., Figure 1b). As in Ditchek, Corbosiero, et al. (2019), tendency values colder than the lowest 25% of the PDF (<−3.82 K; Figure 1b) are defined as significant cloud top cooling grid points.

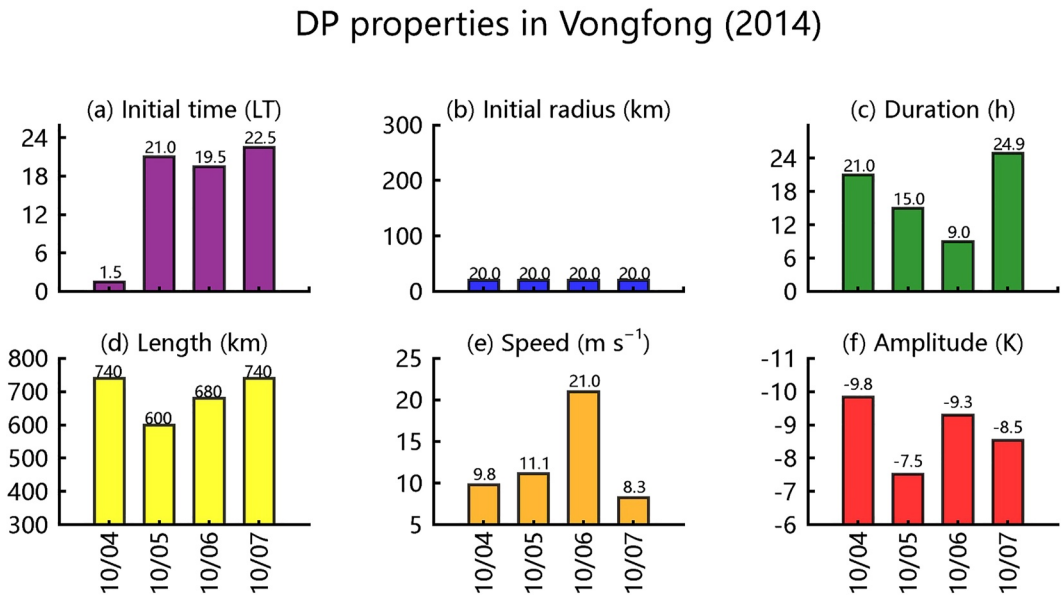

Figure 2. Properties of diurnal pulse (DP) events identified in Super Typhoon Vongfong during 4–7 October 2014, including (a) initial time, (b) initial radius, (c) time duration, (d) length, (e) speed, and (f) amplitude.

4. Identify propagation events (e.g., Figure 1c): All neighboring significant cloud top cooling grid points are identified. When a grouping of at least 15 neighboring grid points occurs, they are identified as a cluster. On a given day, if only one cluster initiates between 00 and 24 LT, that cluster is identified as a propagation event. If more than one cluster initiates on a given day, then the largest cluster is identified as a propagation event.

Figure 1 depicts how this algorithm is applied using Super Typhoon Vongfong (2014) as a representative example. The azimuthally averaged IR BT tendency is given in Figure 1a. Following the convention established in Dunion et al. (2014), warm colors depict cloud-top cooling and cool colors depict cloud-top warming. Multiple instances of outward propagation of cooling cloud tops are observed. By applying the algorithm to Figure 1a, propagation events are objectively identified (Figure 1c). Significant cloud top cooling grid points, determined by the threshold applied in Figure 1b, are indicated by red and yellow dots (Figure 1c). Clusters of significant cloud-top cooling grid points are identified as propagation events (red dots). Also identified (yellow dots) were significant cloud top cooling grid points that either: (a) did not meet the cluster threshold, or (b) were not chosen as the propagation event since a larger cluster was present on that day. The remaining grid points (blue dots) did not have significant cloud top cooling.

For each propagation event, multiple parameters are derived. First, the propagation path is defined as the least square-fitted line through all neighboring significant cloud-top cooling grid points in the identified cluster (e.g., the black lines in Figure 1c). Then, the initial and ending time/location, duration, propagation length, propagation speed, and amplitude are calculated. The duration and propagation length are derived from the differences of time and radius between the initial and ending location of the pulse path, respectively. Propagation speed is calculated by dividing the propagation length by the duration. Finally, the amplitude is defined as the average IR BT tendency of all significant cloud-top cooling grid points belonging to an individual propagation event in the time-radius field (i.e., all red grid points associated with an individual black line in Figure 1c).

Since the DP is considered as a sustained cold-cloud propagation for several hundred kilometers, a propagation event with duration $\geq$6 hr and length $\geq$300 km is defined as a DP event in this study. Propagation events that do not meet these thresholds are defined as non-DP events. Figure 2 shows the distributions of the aforementioned parameters for the DP events identified in Super Typhoon Vongfong (2014). DPs are further classified into on-the-clock DPs (in phase with the diurnal clock defined by Dunion et al., 2014) and off-the-clock DPs (out of phase with the diurnal clock). DPs are classified as on-the-clock DPs when their propagation paths (e.g., black lines in Figure 1c) match the radial locations defined by the diurnal clock (i.e., within $\pm$100 km during each 3-hr clock period). Note that on-the-clock DPs are not required to initiate from the inner core, that is, DPs initiated

Table 3
Number of On-The-Clock DPs From 2001 to 2018 in all Global TCs and the Four Main TC-Prone Basins Along With Their Frequency Relative to the Total Number of DPs in Each Basin

	Global	NWP	SI	NEP	NA
ALL	2,804 (79.7%)	1,023 (85.4%)	548 (78.9%)	589 (76.4%)	308 (69.1%)
TD	467 (76.1%)	151 (83.4%)	90 (73.8%)	127 (73.0%)	28 (60.9%)
TS	1,047 (78.7%)	331 (86.6%)	247 (80.5%)	203 (73.0%)	121 (62.4%)
CAT 1–2	686 (84.4%)	271 (89.4%)	110 (85.3%)	147 (81.2%)	81 (73.6%)
CAT 3–5	603 (79.2%)	267 (80.4%)	100 (73.0%)	109 (79.0%)	81 (84.4%)

further outward but lining up with the diurnal clock are also accounted as on-the-clock DPs, as these DPs may initiate in the inner region but would not be identified until their cooling amplitude increased further radially outward. DPs that do not follow the diurnal clock at all are then defined as off-the-clock DPs. The number and percentage of on-the-clock and off-the-clock DPs are listed in Table 3.

4. Results

4.1. Diurnal Pulse Properties

There are 3,518 DP events identified out of 6,778 TC days during 2001–2018, yielding a DP frequency of 51.9% (Table 1). This global DP frequency is close to the one obtained using a different DP identification method based on the diurnal pulse clock (Ditchek, Corbosiero, et al., 2019; Zhang & Xu, 2021b). Generally, DP propagation length linearly increases with DP duration (Figure 3a). The mean lengths of DPs that lasted 6–9 hr, 9–12 hr, and 12–15 hr are approximately 350 km, 400 km, and 500 km, respectively. Meanwhile, DP propagation speed linearly decreases with DP duration, where the average DP's propagation speed gradually decreases from 15 m s^{-1} to 7 m s^{-1} as the duration increases from 6–9 hr to 27–30 hr (Figure 3b). While DPs > 15 hr mostly propagate at speeds similar to the tropospheric internal inertial gravity waves (5–10 m s^{-1}) in simulation studies (Navarro & Hakim, 2016; Navarro et al., 2017; O'Neill et al., 2017), shorter-duration pulses have a larger variability of length and speed.

The DP frequency shows significant spatial variability across basins (Figure 4 and Table 1). Of all the basins, the NWP shows the highest DP frequency (60%–80% in the tropical NWP < 15° N; Figure 4a). In contrast, the NEP has the lowest DP frequency, especially >15°N where the DP frequency is mostly less than 10% (Figure 4a). DPs have a greater likelihood to occur over open oceans (e.g., the NWP and NA) than over regions more enclosed by land (e.g., the Gulf of Mexico and the South China Sea). Some local maxima are found over coastal waters (e.g., offshore areas over northern South America and eastern South Africa), possibly due to the influence from frequent coastal convection. However, overland samples (IR BT grid points) account for less than 10% of the total sample (see Table S2 in Supporting Information S1). Therefore, as mentioned previously, land effects (e.g.,

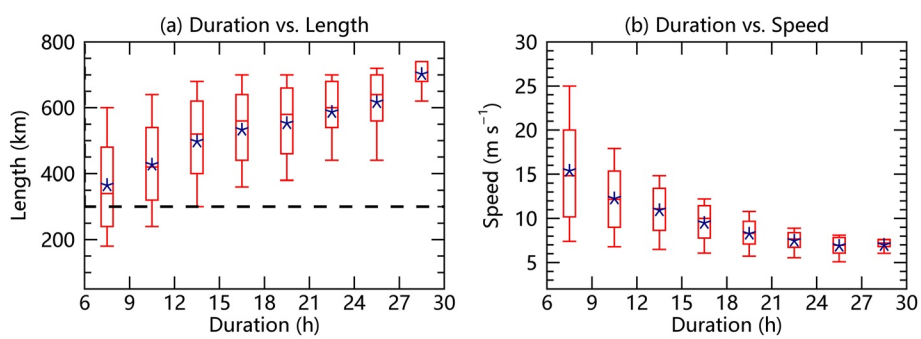

Figure 3. Diurnal pulse (DP)-event (a) propagation length (km) and (b) propagation speed (m s^{-1}) as a function of duration (h) in global tropical cyclones (TCs) from 2001 to 2018. Whiskers, boxes, lines, and blue asterisks are the upper and lower bounds (90%, 10%), interquartile range (75%, 25%), median (50%), and mean values, respectively. DP duration is greater or equal to the value of the *x*-axis coordinate left of the box and less than the value right of the box. The dashed line in (a) marks the 300-km threshold for DP classification. The *x*-axis in both (a) and (b) begins at the 6-hr threshold for DP classification.

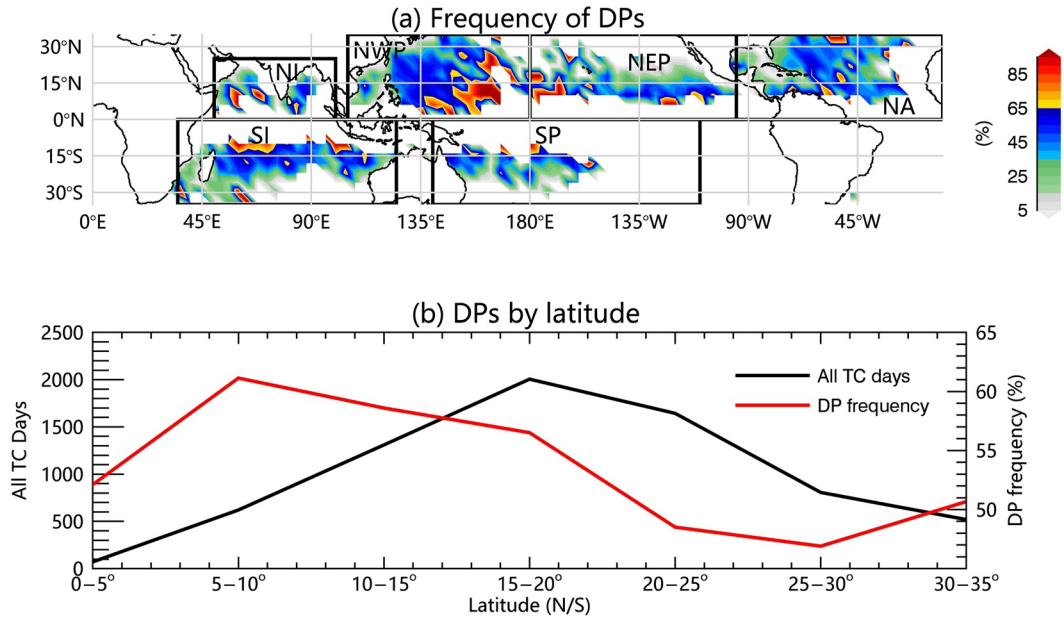

Figure 4. (a) The global distribution of the diurnal pulse (DP) frequency. (b) The number of tropical cyclone (TC) days (black) and the frequency of DP events (red) as a function of the latitude.

coastal convection) had minimum impact on the statistics in this study (Figures S1–S3 in Supporting Information S1). DP frequency is further calculated as a function of latitude (Figure 4b). TCs at low latitudes between 5 and10°N/S are the most likely (~60%) to produce DPs and DP frequency decreases markedly to ~40% at 25° – 30°N/S (Figure 4b). DP frequency is further examined as a function of the TC intensity (Table 1), as previous studies showed that intense TCs are more likely to produce DPs (Ditchek, Corbosiero, et al., 2019; Dunion et al., 2014, 2019). The DP frequency increases with TC intensity from 37% in TDs to 67% in CAT 3–5 hurricanes globally, consistent with previous studies over the NA (Ditchek, Corbosiero, et al., 2019; Ditchek, Molinari, et al., 2019). However, there are significant regional differences in DP frequency at the same intensity level, especially for TCs with weaker intensity (TD–TS). For example, TDs to CAT1–2 hurricanes have the highest DP frequency in the NWP compared to the other TC-prone basins (SI, NEP, NA).

The climatological characteristics of DPs are first analyzed globally and then compared among the four basins (i.e., NWP, SI, NEP, NA). Figure 5 shows the PDF and cumulative distribution (CDF) of DP duration and propagation length. DPs lasting 9–15 hr have the highest frequency, accounting for 42% of the total DP population globally (Figure 5a). DPs lasting longer than 18 hr are less frequent but still contribute a significant fraction of DPs (~25%, Figure 5b). There are ~8% DP events lasting longer than 1 day (24–30 hr). DP duration shows little regional variation, except that the NWP has a slightly higher frequency of DP events lasting 15–24 hr than other basins (Figures 5a and 5b). The global DP propagation length spans from 300 to 800 km with no significant peak of frequency (Figure 5c). Of note is that 18% of DPs propagate as far as 700–800 km. As the maximum radial length propagation has been set to 800 km in this study, some DPs (<5%) propagate even further outward. The DP propagation length varies significantly across basins. The length of DPs in the NWP and NA peaks at 600 km, compared to a maximum at 400 km in the NEP and SI (Figure 5c). The median DP lengths in the NWP/NA and NEP/SI are 580 and 500 km, respectively (Figure 5d).

The timing and location (i.e., radius) where DPs initiate are further examined (Figure 6). DP initiation is the most frequent (~25%) at 03–06 LT and more than half of DPs initiate at midnight to early morning (00–09 LT, Figure 6a). Though DP initiation is less likely in the afternoon, ~40% of DPs do initiate from the afternoon to evening hours (Figure 6a). This result is somewhat different from the diurnal pulse clock in Dunion et al. (2014), which proposed DPs in mature hurricanes primarily develop in the early morning. Most (~75%) DPs originate from the TC's inner region (0–200 km), with 60% initiating within the inner core (i.e., 0–100 km; Figure 6b). There are subtle regional variations in the initial time and location of DPs among the four TC basins examined. For example, more than 50% of DPs in the NWP/NEP/NA initiate at 00–09 LT, but less than 40% do in the SI

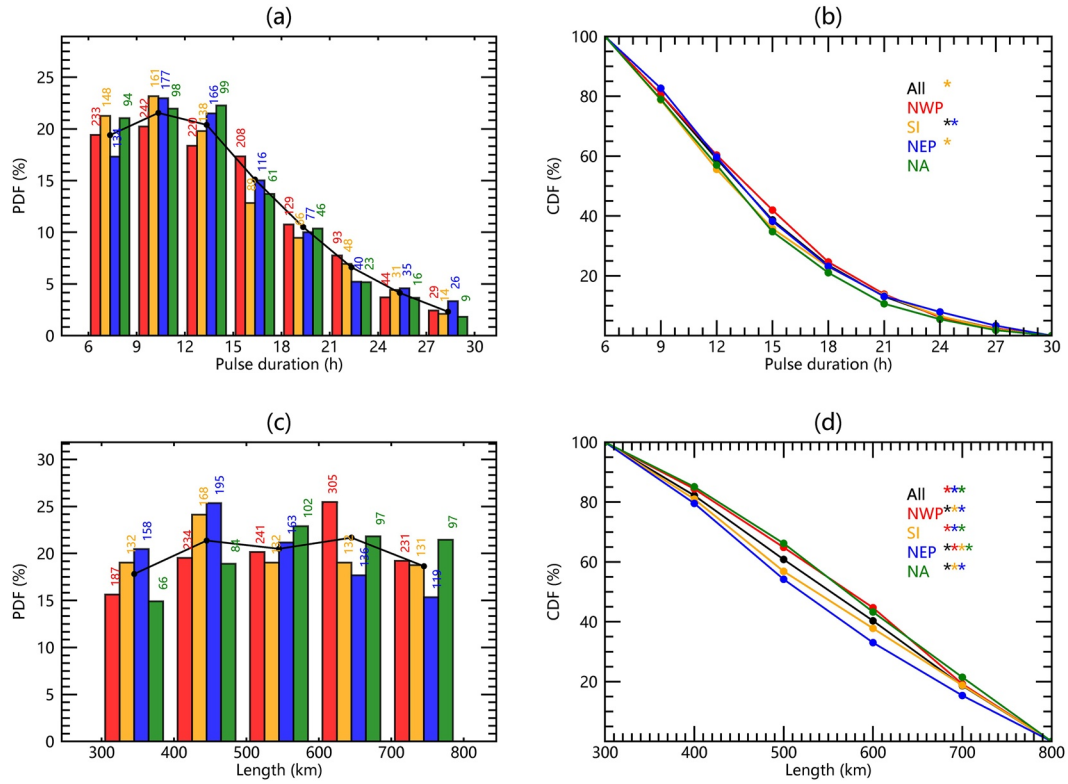

Figure 5. (a) Probability distribution function (PDF) and (b) cumulative distribution function (CDF) of duration in diurnal pulse (DP) events (i.e., duration ≥ 6 hr, length ≥ 300 km) for all basins (black lines) and tropical cyclones (TCs) in the Northwest Pacific (NWP, red), South Indian Ocean (SI, yellow), Northeast Pacific (NEP, blue), and North Atlantic (NA, green) basins. (c, d) Same as (a, b) but for the PDF and CDF of DP propagation length. Event samples are marked at the top of each bar in (a, c). DP properties in (a, c) are greater or equal to the value of the *x*-axis coordinate left of the bar and less than the value right of the bar. Asterisks in (b, d) indicate the DP distribution is significantly different from basin(s) associated with the color(s) of the asterisk(s) at 95% confidence level by the Wilcoxon rank-sum test.

(Figure 6a). Also, DPs in the NEP/NA/SI have a higher likelihood (>60%) of originating in the inner core than the NWP (~50%). In short, DPs are the most likely to develop in the early morning hours within the TC inner core.

In order to examine the relationship between DP initiation and inner-core deep convection, the diurnal cycle of the inner-core (0–100-km) convection is further examined here. Figures 6c and 6d show the cloud top cooling and cold-cloud coverage in the inner core during days with DPs. Both the cloud-top cooling rate (Figure 6c) and cold-cloud coverage (Figure 6d) maximize at 03–06 LT, likely due to the enhancement by nighttime cloud-top radiative cooling and cloud-free sky differential radiative cooling (Ruppert and Hohenegger, 2018). The diurnal cycle phase of inner-core convection is consistent with the initiating time of DPs, suggesting DP initiation is closely related to the development of inner-core deep convection.

The propagation speed of DPs is given in Figure 7a. DPs with a propagation speed of 7–13 m s^{-1} account for more than half of the global DP population (Figure 7a), consistent with previous studies based on either satellite observations or model simulations (Ditchek, Corbosiero, et al., 2019; Dunion et al., 2019; Navarro & Hakim, 2016; O'Neill et al., 2017). The speed of DPs is similar to the speed of internal inertial gravity waves in a rotating, stably stratified atmosphere as in simulation studies (Navarro & Hakim, 2016; Navarro et al., 2017; O'Neill et al., 2017), which may suggest DPs closely resemble inertial gravity waves. Slow (<5 m s^{-1}) and fast (>21 m s^{-1}) propagating DPs occur less than 5% of the time, respectively. Recall that DPs of 6–9 hr (10–20 m s^{-1}) seem to travel faster than longer DPs (5–10 m s^{-1}; Figure 3b). There is also regional variability in the DP propagation speed. NWP DPs travel the fastest (on average 13 m s^{-1}) and DPs in the NEP travel the slowest (on average 11 m s^{-1}).

The pulse amplitude (i.e., 6-hr cloud top cooling rate) is given in Figure 7b. More than half of global DPs produce a cooling amplitude of −6 to −10 K, while less than 10% of DPs have a cooling amplitude greater than −14 K. All basins share a similar mean DP amplitude (on average −9 K) with no significant variability across basins. Interestingly, the

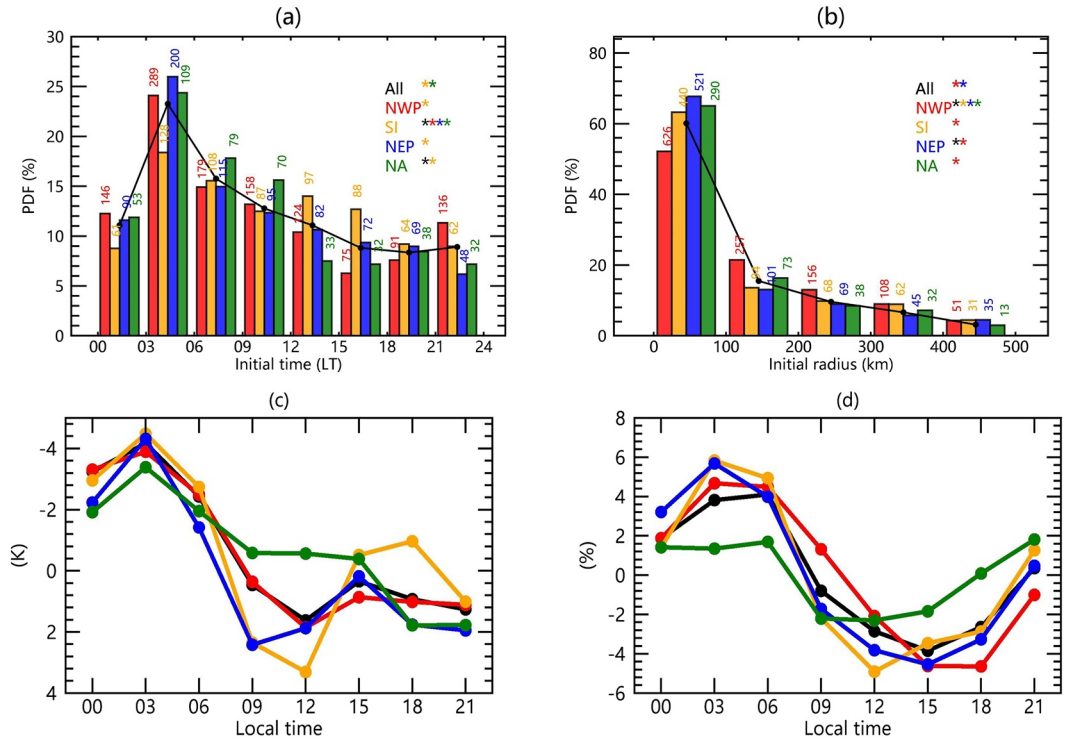

Figure 6. Probability distribution function (PDF) of the (a) initial time and (b) initial radius of diurnal pulse (DP) events (duration ≥ 6 hr, length ≥ 300 km) for all basins (black lines) and tropical cyclones (TCs) in the Northwest Pacific (NWP, red), South Indian Ocean (SI, yellow), Northeast Pacific (NEP, blue), and North Atlantic (NA, green) basins. Event samples are marked at the top of each bar. The anomaly relative to the daily mean of the (c) inner core (0–100 km) IR BT cooling rate (k) and (d) inner-core very cold-cloud (IR BT < 208 K) coverage (%) is given as a function of local time (LT) on DP days. DP properties in (a, b) are greater or equal to the value of the x-axis coordinate left of the bar and less than the value right of the bar. Asterisks in (a, b) indicate the DP distribution is significantly different from basin(s) associated with the color(s) of the asterisk(s) at 95% confidence level by the Wilcoxon rank-sum test.

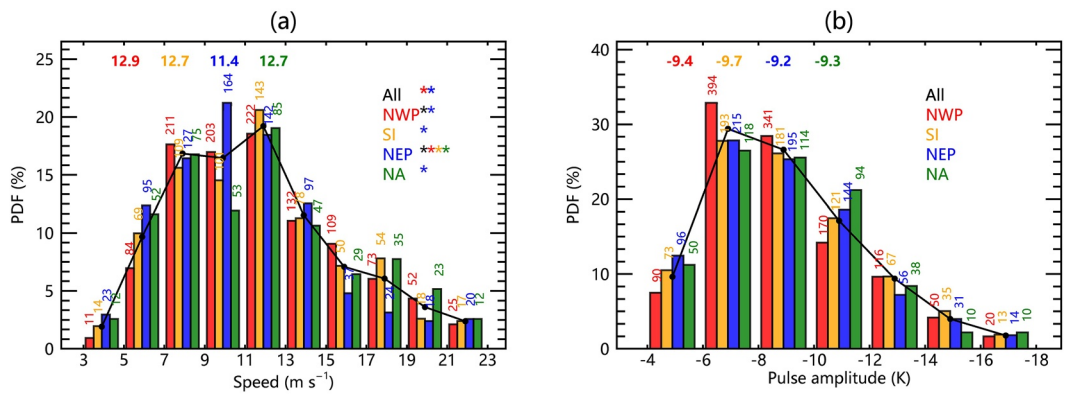

Figure 7. Probability distribution function (PDF) of the (a) propagation speed and (b) amplitude in diurnal pulse (DP) events (duration ≥ 6 hr, length ≥ 300 km) for all basins (black lines) and tropical cyclones (TCs) in the Northwest Pacific (NWP, red), South Indian Ocean (SI, yellow), Northeast Pacific (NEP, blue), and North Atlantic (NA, green) basins. Event samples are marked at the top of each bar. The mean speed and amplitude are marked at the top of (c, d), respectively. DP properties are greater or equal to the value of the x-axis coordinate left of the bar and less than the value right of the bar. DPs with values beyond the rightmost value of the x-axis are not shown. Asterisks indicate the DP distribution is significantly different from basin(s) associated with the color(s) of the asterisk(s) at 95% confidence level by the Wilcoxon rank-sum test.

NWP has the lowest fraction of DPs with strong cooling amplitude (−10 K), possibly because NWP DPs have the longest duration and length (Figure 5), such that the amplitude is smoothed by a large number of cooling grid points.

While DP characteristics are generally consistent with diurnal patterns reported in previous studies (Ditchek, Corbosiero, et al., 2019; Dunion et al., 2014), some cases may not follow the diurnal pulse clock in Dunion et al. (2014) in terms of their onset timing, initial location, length, and speed. The percentages of on-the-clock pulses show that most global DPs (∼80%) identified in this study are consistent with the diurnal clock (Table 3). The frequency of on-the-clock DPs is higher than that of DPs initiated in the evening to early morning (∼60%, Figure 6a), suggesting that not all on-the-clock DPs initiate from the inner core in the early morning. There are ∼20% DPs initiated later than 09 LT at outer radii (>200 km) also lining up the diurnal clock. The 20% of DPs identified as out of phase with the diurnal clock may initiate at a time entirely different from the diurnal clock or propagate with a super-fast/slow speed. There is also significant regional variability in the fraction of on-the-clock pulses: they are highest in the NWP (85.4%) and lowest in the NA (69.1%). Further, the percentage of on-the-clock DPs generally increases with TC intensity, maximizing in CAT1–2 hurricanes, except for in NA TCs. Off-the-clock DPs will be discussed further in Section 5.

4.2. Cloud, Precipitation, and Lightning Patterns

4.2.1. DPs

The azimuthally averaged, 6-hr IR BT trends of DPs categorized by the pulse duration and initiation radius are given in Figure 8. The outward propagation of the cloud top cooling signal can be recognized clearly in most DP events (Figures 8a–8d), extending from the TC center to 800 km. The longer the pulse lasts, the stronger the cooling signal (Figures 8a–8d). Interestingly, DPs are somewhat disrupted during 09–12 LT regardless of the pulse duration, that is, both the propagation speed and cooling amplitude decrease. The weakening of the pulse occurs in the 200–300-km annulus for DPs < 12 hr and 300–400 km annulus for DPs ≥ 12 hr. This weakening is possibly because shortwave radiative heating increases during 09–12 LT compared to prior hours and, therefore, might suppress the pulse-induced cloud top cooling tendency. Beyond these radii, it has been documented that pulses can take on a squall-like appearance, which could explain the observed reinvigoration.

DP composites are further divided into two groups of DPs based on whether they initiate within the inner (0–200 km, Figures 8e–8h) or outer regions (>200 km, Figures 8i–8l). The two groups account for 75% (inner-region initiated) and 25% (outer-region initiated) of the total number of DPs, respectively. The inner-region initiated DPs produce pronounced cloud-top cooling throughout the pulse lifecycle. The cooling amplitude of these DPs is strongest near the TC center in the early morning. Again, these DPs weaken and slow down during 09–12 LT but reintensify in the afternoon (Figures 8e–8h). They also tend to propagate faster in the outer region (>400 km) of the TC (10–18 m s^{-1}) than in the inner region (5–10 m s^{-1}). Similarly, Ditchek, Corbosiero, et al. (2019) reported that the propagation speed of DPs over the Atlantic Ocean is about 8 m s^{-1} and 14 m s^{-1} in the range of 200–350 km and 350–500 km, respectively. The outer-region initiated DPs (Figures 8i–8l) are weaker than the inner-region initiated DPs and their cooling signal is mainly found in the outer rainband (>400 km) region during the afternoon hours.

Since inner-region initiated DPs comprise 75% of all DPs and show a marked cloud top cooling signal, time-radius averaged precipitation tendency and WWLLN lightning strikes for these DPs are given in Figure 9. For inner-region initiated DPs shorter than 12 hr, pronounced precipitation enhancement occurs in the early morning and late afternoon, especially in the inner core, but no propagating features are observed (Figures 9a and 9b). Inner-region initiated DPs longer than 12 hr exhibit stronger precipitation enhancement in both the early morning and the late afternoon, and the early morning precipitation signal propagates radially outward (Figures 9c and 9d). The precipitation signal only propagates out to 300 km, however, even for inner-region initiated DPs longer than 15 hr (Figure 9d), far shorter than the associated cloud top cooling signal (Figure 8). For inner-region initiated DP events lasting 6–12 hr (Figures 9e and 9f), lightning maximizes in the inner core (0–100 km) and shows some degree of propagation in the outer-rainband region from 200 to 500 km. Lightning associated with inner-region initiated DPs lasting longer than 12 hr exhibits a clear propagating signal from the 100–200-km annulus to the outer edge of the TC. However, DPs longer than 12 hr have fewer lightning flashes in the inner core than short-duration pulses (<12 hr), suggesting that long-duration pulses may have relatively weaker inner-core convection or microphysical conditions that are less favorable for lightning production (e.g., limited supercooled liquid water).

Composites of 6-hr IR BT trends, 6-hr precipitation trends, and summed lightning flashes of inner-region initiated DPs are further divided into specific basins (Figure 10). Only DPs longer than 12 hr are considered

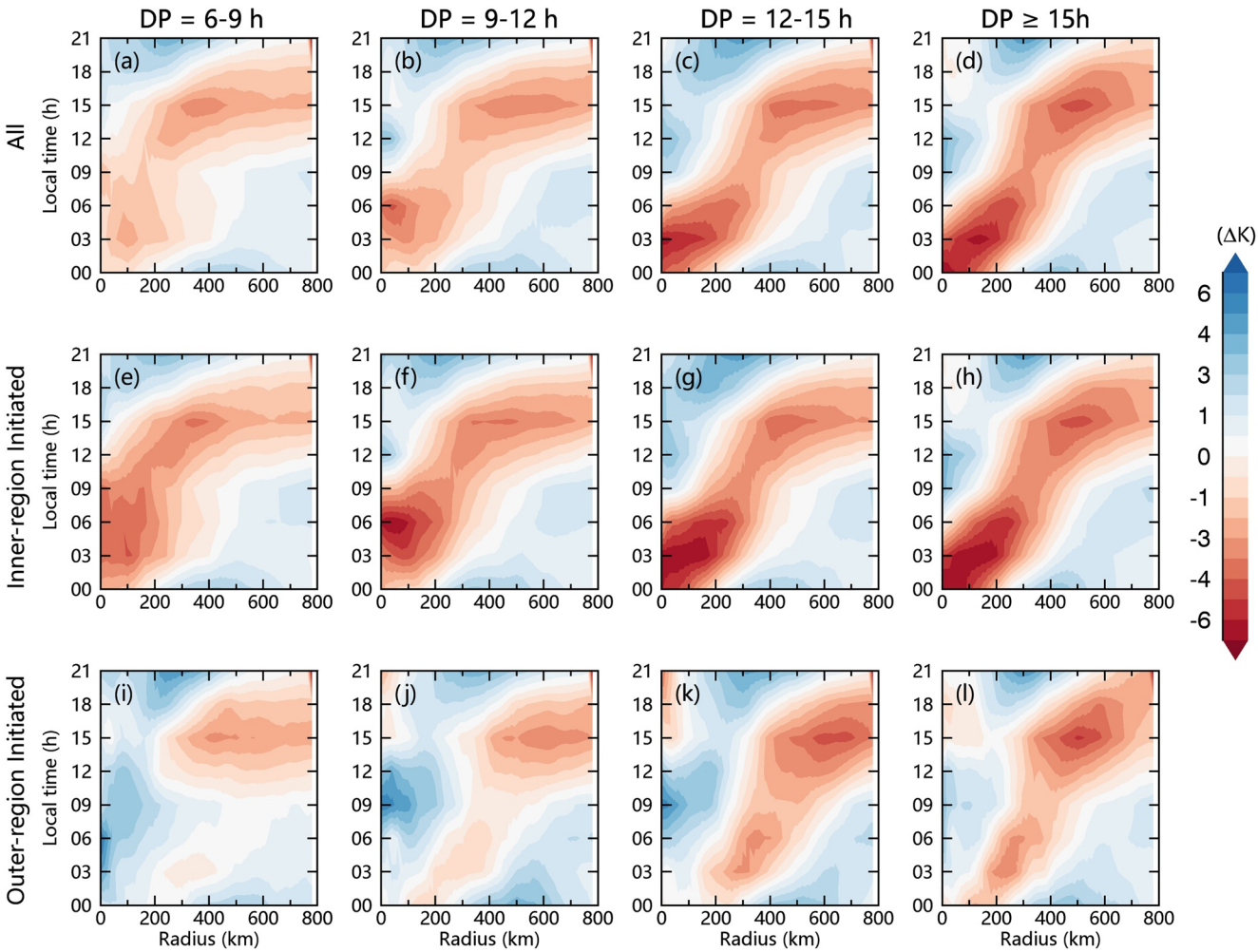

Figure 8. Azimuthally averaged, 6-hr IR BT trends in (a–d) all diurnal pulses (DPs) (duration ≥ 6 hr, length ≥ 300 km), (e–h) inner-region initiated (<200 km) DPs, and (i–l) outer-region initiated (≥200 km) DPs stratified by time duration.

here, since weaker DPs have little regional variability (not shown). In general, inner-region initiated DP events with durations of longer than 12 hr in all four basins display marked propagation signals in cloud-top cooling (Figures 10a–10d). While propagating signals are persistent in most basins, those in the SI are disrupted during 09–12 LT (Figure 10b). In all four basins, the precipitation enhancement signature peaks in the early morning and late afternoon (Figures 10e–10h). The early morning precipitation signal propagates out to about 200–300 km from 00 to 09 LT. TCs in the NA have relatively weak precipitation variations, possibly due to the higher latitude of the NA TCs. The associated lightning distributions vary substantially among basins. Inner-region initiated DPs with durations of longer than 12 hr in the NA produce the most lightning (Figure 10l), consistent with global lightning climatology (Cecil et al., 2014; Virts et al., 2013). In addition, there may be some storms near the coast that produce a large amount of lightning in outer rainbands, as the lightning in NA TCs is reduced in the outer region (400–600 km) after removing data points over land (Figure S3 in Supporting Information S1). The lightning in NA TCs also exhibits the strongest propagation pattern, while other basins show only weak to moderate propagating features (Figures 10i–10l).

4.2.2. DPs Versus Non-DPs

One of the main questions this study aims to answer is how the daily mean TC structure varies between days with and without a DP. Here, the daily mean IR BT, precipitation, and lightning density of TCs on DP days are subtracted from days without DPs and are stratified by initial classification into TD, TS, CAT 1–2, and CAT 3–5 (Figure 11). Cold clouds, precipitation, and lightning are all markedly enhanced on DP days of the same

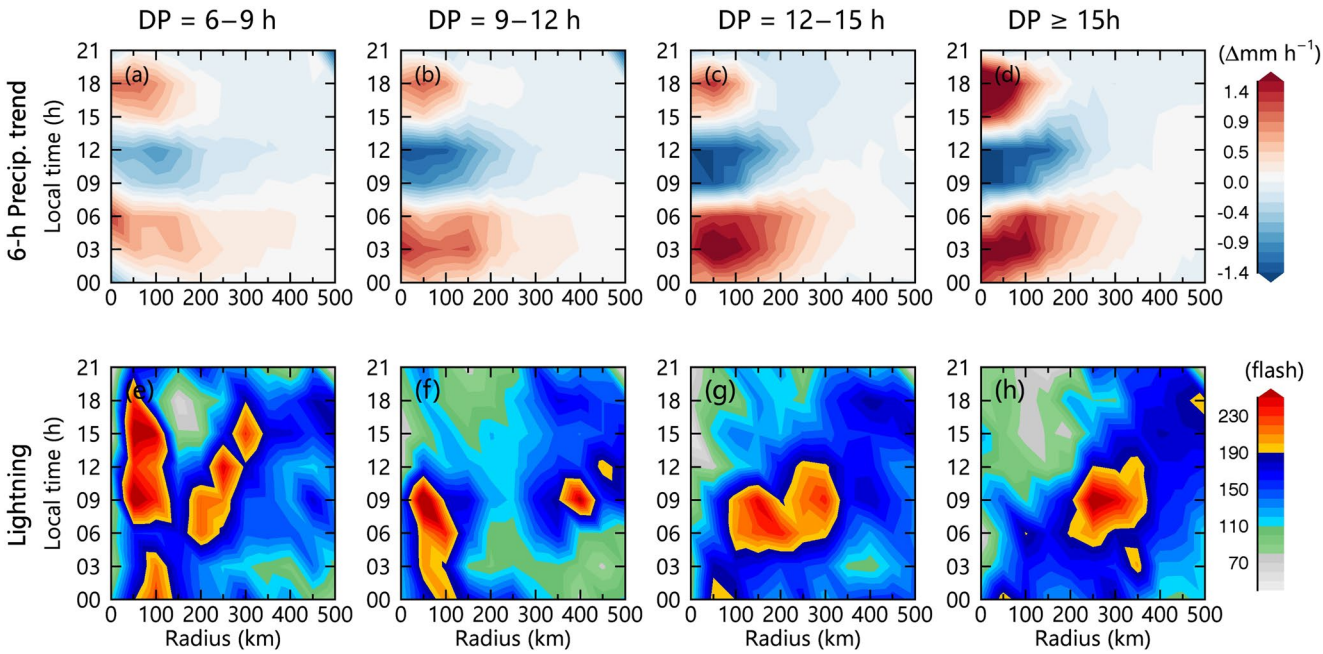

Figure 9. Azimuthally averaged 6-hr precipitation trends (a–d) and summed lightning flashes (e–h) for diurnal pulse (DP) events of different time durations for inner-region initiated DP events (i.e., <200 km), only.

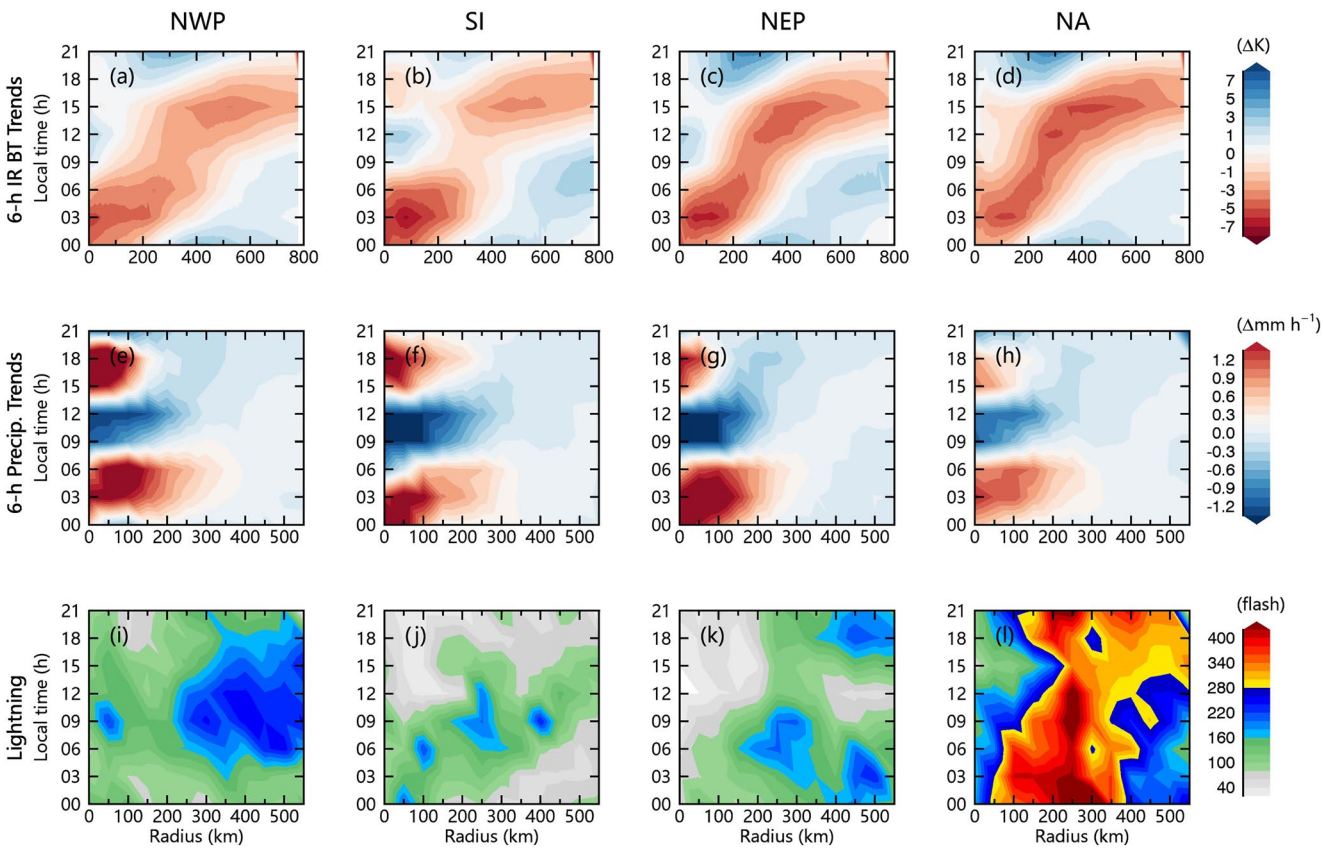

Figure 10. Azimuthally averaged (a–d) 6-hr IR BT trends, (e–h) 6-hr precipitation trends, and (i–l) summed lightning flashes for tropical cyclones (TCs) in (a, e, i) the Northwest Pacific (NWP), (b, f, j) South Indian Ocean (SI), (c, g, k) Northeast Pacific (NEP), and (d, h, l) North Atlantic (NA) for inner-region initiated (i.e., <200 km) diurnal pulse (DP) events lasting longer than 12 hr.

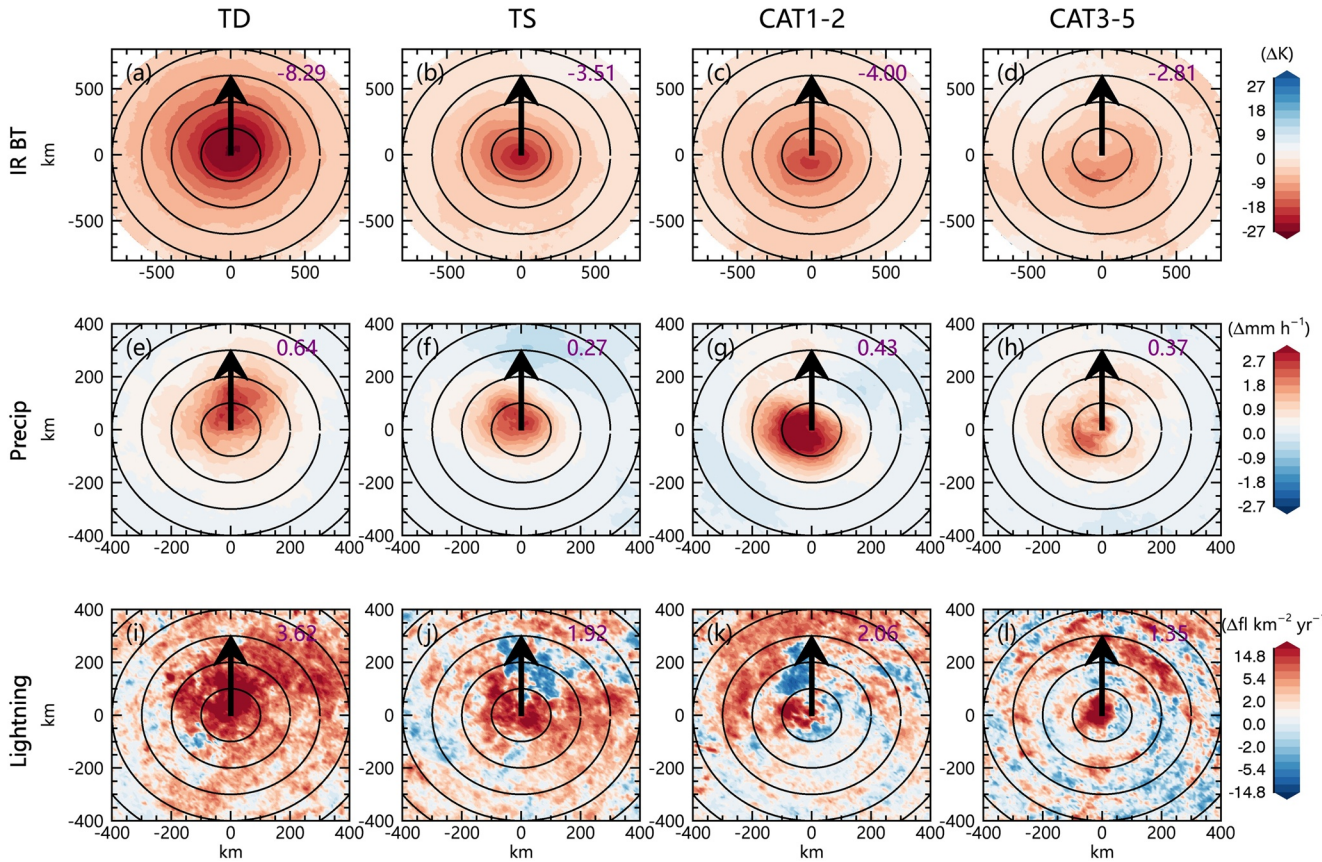

Figure 11. Difference of daily mean (a–d) IR BT, (e–h) precipitation, and (i–l) lightning between tropical cyclones (TCs) with and without diurnal pulses (DPs) and as a function of TC intensity (TD, TS, CAT 1–2, CAT 3–5). Composites are rotated relative to the environmental vertical wind shear vector between 850 and 200 hPa (black arrow). The mean difference of the 0−600-km area is marked at the upper right corner.

TC intensity. While the cloud-top cooling on DP days extends around a broad area of the TC, the maximum enhancement of precipitation and lightning mostly occurs in the downshear-left quadrant of the inner core. The precipitation enhancement and convective invigoration (lightning) likely increase latent heating (due to condensation) in the inner core, enhance the warm-core structure (subsidence from deep convection), and enhance the TC vortex (by vertical stretching), which are favorable for TC intensification (Rogers et al., 2016; Stevenson et al., 2014, 2018; Susca-Lopata et al., 2015). All of these enhancements are most evident in weak TCs (TD/TS) rather than in strong TCs (CAT 3–5), suggesting that DPs may have more impact on developing TCs rather than mature TCs. In fact, Zhang & Xu (2021b) reported a positive relationship between DP activity and TC intensification—rapidly intensifying TCs are more likely to produce DPs, and DPs have a longer duration on the day before, or during, TC rapid intensification.

4.3. Environmental and TC Convective Factors

The potential relationships between the DPs, environmental conditions, and internal structures (variables defined in Table 2) are examined to determine important factors impacting DPs. Mean values of these variables during the most common initiation time (00–03 LT; Figure 6a) on days with and without DPs are shown in Table 4. DP events occur in TCs of stronger intensity and more intense inner-core (0–100-km) convection, such as higher and more extended cold-cloud tops (IR BT, cold-cloud coverage) and greater cloud top cooling trends (−3.4 K) within the inner core. DP events also prefer environments with warmer SST (~29°C), lower shear (~9 m s^{-1}), and a moister troposphere. Such large-scale environments of DPs are no doubt favorable for TC intensification and development of deep convection. Almost all variables show statistically significant differences between DPs and non-DPs, and DPs and All days, at the 95% confidence level of the student's *t*-test (except the intensity between DPs and All days). These results are similar to those found in Table 1 of Ditchek, Corbosiero, et al. (2019), where enhanced

Table 4
Mean Values of Environmental and Convective Factors From 00 to 03 LT on DP, Non-DP, and all Days

Variables	DP (x)	Non-DP (*)	All (+)
Intensity (kt)	53.2*	48.7^{+x}	51.2*
IR BT (K)	222.0^{*+}	236.6^{+x}	229.6^{*x}
IR BT 6-hr trend (K)	-3.4^{*+}	1.7^{+x}	-0.7^{*x}
Cold-cloud coverage (%)	46.0^{*+}	32.0^{+x}	38.5^{*x}
SST (°C)	29.0^{*+}	27.7^{+x}	28.4^{*x}
Shear (m s^{-1})	9.3^{*+}	11.4^{+x}	10.2^{*x}
RH mid-upper (%)	53.8^{*+}	47.2^{+x}	50.9^{*x}
RH low-middle (%)	67.5^{*+}	59.0^{+x}	64.1^{*x}

Note. Student's *t*-tests are performed to examine the significance of the differences at the 95% confidence level. Statistically significant differences between each of the three individual groups (i.e., DP, non-DP, and All) are indicated by x, *, and +, respectively.

deep convection in the inner core and an overall favorable environment for deep convection were found overnight on days with long-lived cooling pulses.

The same environmental and TC convective factors are also compared across the TC-prone basins. Figure 12 shows the mean values of the environmental variables (at 00–03 LT) on DP days, non-DP days, and overall. Significant regional variability is found in the environmental conditions of the basins. Overall, the NWP, where DPs are the most frequent (Table 1), has the highest SST, lowest shear, and the highest mid-upper-level and low-level relative humidity (black dots in Figure 12). This finding suggests that environmental conditions favorable for TC intensification also promote DP development. On the contrary, environmental conditions in the NEP are the least favorable for TC intensification (i.e., the coldest SST, a relatively dry troposphere, and the second strongest shear). This basin has similar characteristics to the NA, though the NA has a much stronger shear, overall. When DPs do develop, the SST is elevated compared to non-DP days, especially in colder basins (NEP and SI; Figure 12a), possibly because weakening TCs are less likely to produce DPs and the weakening phase is usually over cooler SST. Additionally, the shear is weaker on DP days in all basins except the NEP (Figure 12b). Mid-to-upper-level RH is thought to be an important factor in the TC diurnal oscillation, since a moister environment could prevent deep convection from dry air entrainment (Ditchek, Corbosiero, et al., 2019; Knaff et al., 2019). Here, the mid-to-upper-level RH is 5–8% higher on DP days in the NWP, SI, and NEP basins, but changes little in the NA (Figure 12c). Additionally, the difference in the low-level RH between DP and non-DP days is minor in all basins except the NEP (Figure 12d). DPs still occur even under strong shear and dry conditions (e.g., in the NA), suggesting SST dominates humidity and shear in DP development.

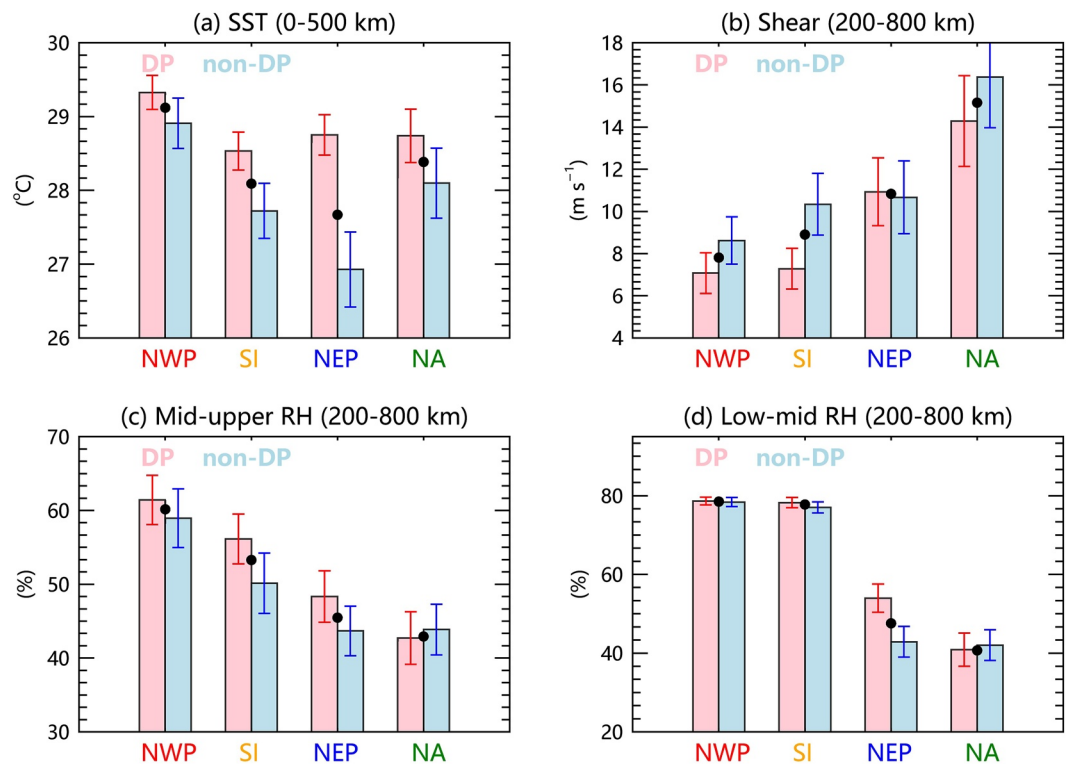

Figure 12. Mean values of (a) sea surface temperature (SST), (b) vertical wind shear, (c) mid-upper relative humidity, and (d) low-midrelative humidity at the initial time of the day (00–03 LT) for diurnal pulse (DP) days (red bars) and non-DP days (blue bars) in Northwest Pacific (NWP), South Indian Ocean (SI), Northeast Pacific (NEP), and North Atlantic (NA) tropical cyclones (TCs). The black dots represent the mean value of all TC days in each basin. Error bars are 0.5 standard deviations.

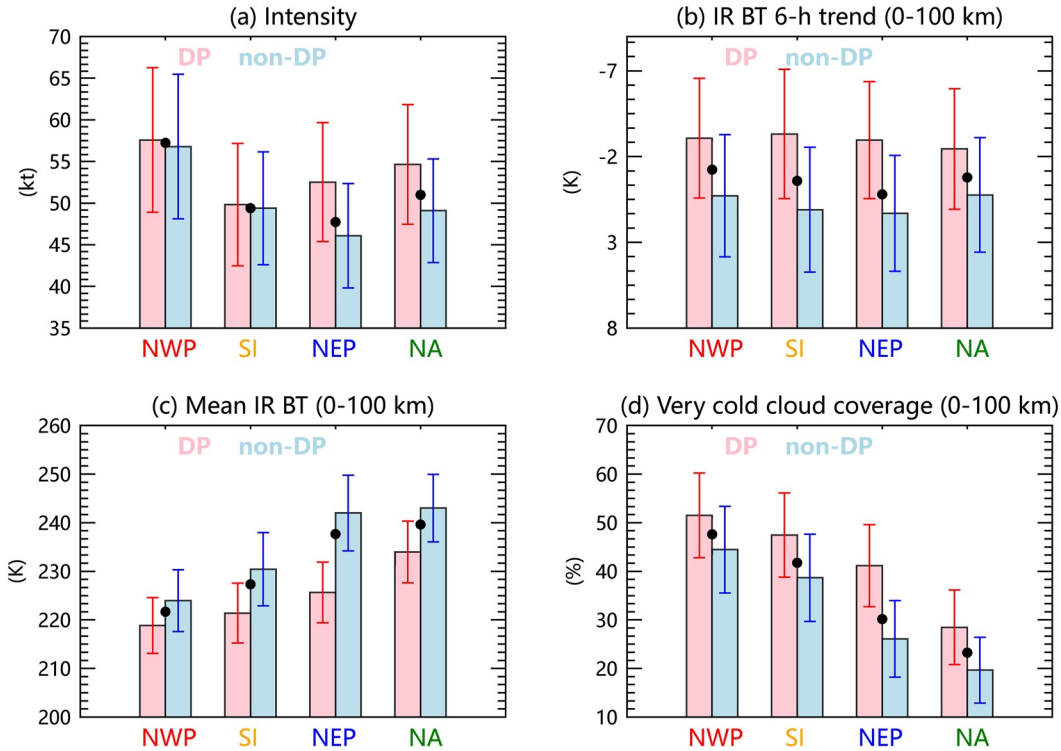

Figure 13. The same as Figure 12, but for mean values of (a) tropical cyclone (TC) intensity, (b) 6-hr IR BT trend, (c) mean IR BT, and (d) the coverage of very cold clouds (IR BT < 208 K).

Figure 13 depicts the mean values of the TC convective variables (at 00–03 LT) on DP days, non-DP days, and overall. On average, NWP TCs have the strongest intensity, the coldest inner-core cloud tops, and the largest coverage of very cold clouds (IR BT < 208 K). Interestingly, TC intensity exhibits an inconsistent tendency between DP and non-DP days in different basins (Figure 13a). TCs in the NEP and NA are notably stronger on DP days than on non-DP days, consistent with conclusions in previous studies (Ditchek, Corbosiero, et al., 2019; Ditchek, Molinari, et al., 2019). Conversely, TCs with DPs in the NWP and SI have little difference in intensity compared to TCs without DPs (Figure 13a). Furthermore, DP events have a markedly greater cloud top cooling rate (Figure 13b), colder cloud tops (mean IR BT; Figure 13c), and larger coverage fraction of very cold clouds (IR BT < 208 K; Figure 13d) within the inner core regardless of basin, suggesting that inner-core deep convection is likely a critical factor in triggering a DP.

5. Conclusions and Discussion

Although DPs in the upper-level clouds of TCs have been well recognized (Ditchek, Corbosiero, et al., 2019; Ditchek, Molinari, et al., 2019; Ditchek et al., 2020; Kossin, 2002), the characteristics of DPs in global TCs have not been thoroughly investigated. This study, therefore, documents the overall and regional variability of DPs worldwide from 2001 to 2018 using an objective metric that identifies DPs in TCs using a framework in which the pulse is not required to follow the temporal phase of the diurnal pulse clock (Dunion et al., 2014). Although taking a different approach to identify DPs, the composite features of the pulse are generally consistent with previous studies (e.g., Ditchek, Corbosiero, et al., 2019; Ditchek, Molinari, et al., 2019; Dunion et al., 2014). Both the global and regional properties of DPs are quantified, including the initial and ending time/location, duration, propagation length, propagation speed, and amplitude. Additionally, by combining long-term satellite-based IR BT data, a multi-satellite precipitation product, and ground-based lightning observations, the environmental conditions and internal convective structures of the DP are analyzed.

The main conclusions of this study are summarized as follows:

1. DP events occur 52% of the time in global TCs. TCs at lower latitudes ($5-10°$) and over the open ocean are more likely to produce DPs. DPs are the most frequent in the NWP, occurring on 60% of all TC days in that

region. The NWP also has the largest fraction of DPs worldwide (34%). In contrast, the regional mean DP frequency is the lowest in the NEP (42%), with the NA (54%) and SI (51%) in between. About 80% of the global DPs identified in this study follow the diurnal pulse clock proposed by Dunion et al. (2014), while 20% of the DPs are out of phase with the diurnal pulse clock. The frequency of on-the-clock DPs was highest in the NWP (85%) and lowest in the NA (69%).

2. The median duration of DPs is 12–15 hr, with 25% of DPs lasting longer than 18 hr. DP duration varies little across basins except for the slightly longer duration of DPs in the NWP. The median distance that DPs propagate is 500–600 km and 18% of the DPs propagate as far as 700–800 km. The frequency of DP length peaks at 600 km in the NWP and NA compared to 400 km in the SI and NEP.
3. The propagation speed of DPs decreases with the increase of duration. The mean propagation speed of all DPs is 11–13 m s^{-1} and very long-lived (>15 hr) DPs propagate at a speed similar to tropospheric internal inertial gravity waves in simulation studies (~10 m s^{-1}) (Navarro & Hakim, 2016; O'Neill et al., 2017). NWP DPs travel the fastest (mean ~13 m s^{-1}) and DPs in the NEP the slowest (~11 m s^{-1}). DP cloud top cooling rates have a maximum frequency between −6 and −8 K (per 6 hr) and all basins share a similar mean DP amplitude (~−9 K). The longer the pulse duration, the stronger the amplitude.
4. Most DPs initiate in the inner core (0–100 km) during nighttime, in phase with inner-core deep convection (Dunion et al., 2014; Navarro & Hakim, 2016; O'Neill et al., 2017; Ruppert & O'Neill, 2019). DPs initiated from the inner region (0–200 km) are notably stronger than DPs initiated in the outer region (≥200 km). Interestingly, the DP signal becomes weaker and slower during 09–12 LT when propagating through the 200–400-km annulus. Precipitation and lightning also display outward propagation for DPs longer than 12 hr, while the precipitation and lightning propagate in the inner (0–200 km) and outer regions (≥200 km), respectively. Inner-core convective clouds, precipitation, and lightning increase notably on DP days and weak TCs have the most significant deep convective enhancement.
5. DPs are more likely to occur in environmental conditions favorable for TC intensification (warmer SST, lower shear, and a moister troposphere). SST is the most important environmental factor impacting the DP, especially in the colder basins (NEP and SI). In contrast, there is little increase in humidity in the NA on DP days, and wind shear differs little between DP and non-DP days in the NEP. On the other hand, DPs are associated with TCs with more vigorous inner-core (0–100-km) deep convection (higher and more extended cold-cloud tops, faster cloud top cooling rate). Pulsing TCs are significantly stronger than TCs with no DPs in the NEP and NA basins; however, the TC intensity varies little in the NWP and SI. These findings suggest that invigorated deep convection within the TC inner core is crucial for DP development regardless of basin.

Several interesting issues are found in this study associated with the mechanism of the DP and its relationship with TC convection, intensity, and environment. Although a DP is the most likely to form in the early morning and near the inner region (0–200 km), there is a considerable number of pulse events that initiate in the afternoon to evening (~40%) and/or outside the inner region (≥200 km, ~25%) as shown in Figure 6. It is possible that some morning-initiated DPs (in the inner core) have weak cooling signature at the beginning but significantly strengthens at the outer radii when propagating outward. In fact, pulses initiated in the outer region are significantly weaker than pulses initiated near the inner region (Figure 8). Additionally, off-the-clock pulses that do not follow the diurnal pulse clock were also found ~20% of the time (Table 3). Similarly, Trabing and Bell (2021) found that three DPs in Super Typhoon Kong-rey (2018) initiated from the inner core during 15–21 LT instead of the early morning, suggesting that pulsing is not diurnally "locked." Since various studies demonstrate that the environments conducive for convective development are also important to the DP (Ditchek, Corbosiero, et al., 2019; Ditchek, Molinari, et al., 2019; Duran et al., 2021; Knaff et al., 2019), the variability of the environment may also change the phase of the diurnal cycle (Ditchek, Corbosiero, et al., 2019; Ditchek et al., 2020; Stevenson et al., 2016; Trabing & Bell, 2021). Ditchek et al. (2020) hypothesized that the environments of off-the-clock cooling pulses may be more favorable for deep convection and facilitate the pulse to initiate earlier. Another hypothesis is that off-the-clock pulses tend to occur in high-shear environments such that the asymmetric convective structure could change the phase of the pulse (Hong et al., 2006; Ditchek, Corbosiero, et al., 2019; Ditchek, Molinari, et al., 2019; Trabing & Bell, 2021). Our study shows that NA TCs have the highest frequency (~30%) of off-the-clock pulses (Table 3). Since NA TCs are in high-shear environments (Figure 12), this result may support the second hypothesis, suggesting that changing the environmental conditions may impact not only the frequency of DPs but also the phase of the diurnal variation.

The pulses in this study are consistent with the interpretation that the DP may be triggered by convectively-driven internal inertial gravity waves (Dunion et al., 2014; Evans & Nolan, 2019; Navarro et al., 2017; O'Neill et al., 2017;

Ruppert & O'Neill, 2019), as pulsing TCs have significantly stronger overnight deep convection within the inner core than TCs with no pulses (Figure 13) and the initial time of pulses is consistent with the peak time of inner-core deep convection (Figure 6). The average propagation speed, especially for long-lived DPs (>15 hr), is similar to the speed of tropospheric internal inertial gravity waves in a rotating, stably stratified atmosphere as in simulation studies (~10 m s^{-1}; Figure 7) (Navarro & Hakim, 2016; O'Neill et al., 2017). However, the DP signal shows inconsistent features between the inner and outer regions, manifested as an evident weakening and decelerating tendency of the pulse signal during 09–12 LT between 200 and 400 km (Figure 8). Interestingly, the precipitation and lightning also propagate in the inner (0–300 km) and outer regions (>200 km), respectively (Figure 9), suggesting the dominant mechanism of the pulse may be different between the inner and outer regions. It is hypothesized, therefore, that the initiation of the DP is triggered by inertia-gravity waves associated with the invigoration of inner-core deep convection (Evans & Nolan, 2019; Navarro et al., 2017; O'Neill et al., 2017; Ruppert & O'Neill, 2019). Conversely, the propagation of the DP in the outer-rainband region may be more dependent on environmental conditions and have tropical squall-line characteristics (Ditchek et al., 2020; Dunion et al., 2019; Trabing & Bell, 2021), such that pulses in more favorable environments (e.g., the NWP) propagate longer and farther from the center. Based on ship-borne observations, Trabing and Bell (2021) also proposed that the DP might not only be driven by inner-core deep convection, but also maintained by the outer-rainband convection in Super Typhoon Kong-rey (2018).

Although this study combines multi-source observations to demonstrate the characteristics of the DP comprehensively, there is a lack of high spatiotemporal resolution data on the thermodynamic and deep convective structures of DPs. Further research is needed using high-resolution aircraft observations or advanced numerical models to examine the structure of the DP in time and space, to improve the understanding of the DP generation, development, and its impact on TC structure.

Data Availability Statement

The IBTrACS data can be accessed from the NOAA National Climatic Data Center (Knapp et al., 2018). The IMERG rainfall product data can be downloaded from NASA Goddard Earth Sciences Data and Information Services Center (Huffman et al., 2019). The Gridded Satellite (GridSat) B1 data can be downloaded from the National Oceanic and Atmospheric Administration (NOAA) Climate Data Record (CDR) program (Knapp et al., 2014). The World Wide Lightning Location Network (WWLLN) lightning data can be subscribed from its website (http://wwlln.net). The ERA5 reanalysis data can be downloaded from the Climate Data Store (Hersbach et al., 2019).

Acknowledgments
This research was supported by the National Natural Science Foundation of China (41975053, 42275054) and the Guangdong Provincial Department of Science and Technology, China (Grants 2019QN01G107, 2019ZT08G090). We sincerely thank the three anonymous reviewers, Editor, and Associate Editor for providing constructive comments and suggestions, which are very helpful for improving this manuscript. We also thank the World Wide Lightning Location Network (http://wwlln.net), a collaboration among over 50 universities and institutions, for providing the lightning location data in this paper. The scientific results and conclusions, as well as any views or opinions expressed herein, are those of the author(s) and do not necessarily reflect those of OAR or the Department of Commerce.

References

Abarca, S. F., Corbosiero, K. L., & Galarneau Jr., T. J. (2010). An evaluation of the worldwide lightning location Network (WWLLN) using the National lightning detection Network (NLDN) as ground truth. *Journal of Geophysical Research*, *115*. D18206. https://doi.org/10.1029/2009JD013411

Bowman, K. P., & Fowler, M. D. (2015). The diurnal cycle of precipitation in tropical cyclones. *Journal of Climate*, *28*(13), 5325–5334. https://doi.org/10.1175/JCLI-D-14-00804.1

Cecil, D. J., Buechler, D. E., & Blakeslee, R. J. (2014). Gridded lightning climatology from TRMM-LIS and OTD: Dataset description. *Atmospheric Research*, *135–136*, 404–414. https://doi.org/10.1016/j.atmosres.2012.06.028

Chen, S., & Cotton, W. R. (1988). The sensitivity of a simulated extratropical mesoscale convective system to longwave radiation and ice-phase microphysics. *Journal of the Atmospheric Sciences*, *45*(24), 3897–3910. https://doi.org/10.1175/1520-0469(1988)045<3897:tsoase>2.0.co;2

DeMaria, M., DeMaria, R. T., Knaff, J. A., & Molenar, D. (2012). Tropical cyclone lightning and rapid intensity change. *Monthly Weather Review*, *140*(6), 1828–1842. https://doi.org/10.1175/MWR-D-11-00236.1

DeMaria, M., Sampson, C. R., Knaff, J. A., & Musgrave, K. D. (2014). Is tropical cyclone intensity guidance improving? *Bulletin of the American Meteorological Society*, *95*(3), 387–398. https://doi.org/10.1175/bams-d-12-00240.1

Desormeaux, Y., Rossow, W. B., Brest, C. L., & Campbell, G. G. (1993). Normalization and calibration of geostationary satellite radiances for the international satellite cloud climatology project. *Journal of Atmospheric and Oceanic Technology*, *10*(3), 304–325. https://doi.org/10.1175/1520-0426(1993)010<0304:NACOGS>2.0.CO;2

Ditchek, S. D., Corbosiero, K. L., Fovell, R. G., & Molinari, J. (2019). Electrically active tropical cyclone diurnal pulses in the Atlantic Basin. *Monthly Weather Review*, *147*(10), 3595–3607. https://doi.org/10.1175/MWR-D-19-0129.1

Ditchek, S. D., Corbosiero, K. L., Fovell, R. G., & Molinari, J. (2020). Electrically active diurnal pulses in Hurricane Harvey (2017). *Monthly Weather Review*, *148*(6), 2283–2305. https://doi.org/10.1175/MWR-D-20-0022.1

Ditchek, S. D., Molinari, J., Corbosiero, K. L., & Fovell, R. G. (2019). An objective climatology of tropical cyclone diurnal pulses in the Atlantic Basin. *Monthly Weather Review*, *147*(2), 591–605. https://doi.org/10.1175/MWR-D-18-0368.1

Dunion, J. P., Thorncroft, C. D., & Nolan, D. S. (2019). Tropical cyclone diurnal cycle signals in a hurricane nature run. *Monthly Weather Review*, *147*(1), 363–388. https://doi.org/10.1175/MWR-D-18-0130.1

Dunion, J. P., Thorncroft, C. D., & Velden, C. S. (2014). The tropical cyclone diurnal cycle of mature hurricanes. *Monthly Weather Review*, *142*(10), 3900–3919. https://doi.org/10.1175/MWR-D-13-00191.1

Duran, E. L., Berndt, E. B., & Duran, P. (2021). Observation of the tropical cyclone diurnal cycle using hyperspectral infrared satellite sounding retrievals. *Monthly Weather Review*, *149*(11), 3671–3690. https://doi.org/10.1175/MWR-D-20-0415.1

Emanuel, K., Chonabayashi, S., Bakkensen, L., & Mendelsohn, R. (2012). The impact of climate change on global tropical cyclone damage. *Nature Climate Change*, *2*(3), 205–209. https://doi.org/10.1038/nclimate1357

Evans, R. C., & Nolan, D. S. (2019). Balanced and radiating wave responses to diurnal heating in tropical cyclone–like vortices using a linear nonhydrostatic model. *Journal of the Atmospheric Sciences*, *76*(8), 2575–2597. https://doi.org/10.1175/JAS-D-18-0361.1

Gray, W. M., & Jacobson, R. W. (1977). Diurnal variation of deep cumulus convection. *Monthly Weather Review*, *105*(9), 1171–1188. https://doi.org/10.1175/1520-0493(1977)105<1171:DVODCC>2.0.CO;2

Guimond, S. R., Heymsfield, G. M., & Turk, F. J. (2010). Multiscale observations of Hurricane Dennis (2005): The effects of hot towers on rapid intensification. *Journal of the Atmospheric Sciences*, *67*(3), 633–654. https://doi.org/10.1175/2009JAS3119.1

Hendricks, E., Peng, M., Fu, B., & Li, T. (2010). Quantifying environmental control on tropical cyclone intensity change. *Monthly Weather Review*, *138*(8), 3243–3271. https://doi.org/10.1175/2010MWR3185.1

Hersbach, H., Bell, B., Berrisford, P., Biavati, G., Horányi, A., Muñoz Sabater, J., et al. (2019). ERA5 monthly averaged data on pressure levels from 1959 to present [Dataset]. Copernicus Climate Change Service (C3S) Climate Data Store (CDS). https://doi.org/10.24381/cds.6860a573

Hersbach, H., Bell, B., Berrisford, P., Hirahara, S., Horányi, A., Muñoz-Sabater, J., et al. (2020). The ERA5 global reanalysis. *Quarterly Journal of the Royal Meteorological Society*, *146*(730), 1999–2049. https://doi.org/10.1002/qj.3803

Hong, G., Heygster, G., & Rodriguez, C. A. M. (2006). Effect of cirrus clouds on the diurnal cycle of tropical deep convective clouds. *Journal of Geophysical Research*, *111*, D06209. https://doi.org/10.1029/2005JD006208

Hou, A. Y., Kakar, R. K., Neeck, S., Azarbarzin, A. A., Kummerow, C. D., Kojima, M., et al. (2014). The global precipitation measurement mission. *Bulletin of the American Meteorological Society*, *95*(5), 701–722. https://doi.org/10.1175/BAMS-D-13-00164.1

Houze, R. A., Rutledge, S. A., Matejka, T. J., & Hobbs, P. V. (1981). The mesoscale and microscale structure and organization of clouds and precipitation in midlatitude cyclones. III: Air motions and precipitation growth in a warm-frontal rainband. *Journal of the Atmospheric Sciences*, *38*(3), 639–649. https://doi.org/10.1175/1520-0469(1981)038<0639:tmamsa>2.0.co;2

Huffman, G. J., Bolvin, D. T., Nelkin, E. J., & Tan, J. (2020). *Integrated Multi-satellitE Retrievals for GPM (IMERG) technical documentation (technical documentation)*. NASA. Retrieved from https://pmm.nasa.gov/data-access/downloads/gpm

Huffman, G. J., Stocker, E. F., Bolvin, D. T., Nelkin, E. J., & Tan, J. (2019). GPM IMERG final precipitation L3 half hourly 0.1 degree x 0.1 degree V06 [Dataset]. Goddard Earth Sciences Data and Information Services Center (GES DISC). https://doi.org/10.5067/GPM/IMERG/3B-HH/06

Hutchins, M. L., Holzworth, R. H., Brundell, J. B., & Rodger, C. J. (2012). Relative detection efficiency of the World Wide lightning location Network. *Radio Science*, *47*, RS6005. https://doi.org/10.1029/2012RS005049

Joyce, R. J., Janowiak, J. E., Arkin, P. A., & Xie, P. (2004). Cmorph: A method that produces global precipitation estimates from passive microwave and infrared data at high spatial and temporal resolution. *Journal of Hydrometeorology*, *5*(3), 487–503. https://doi.org/10.1175/1525-7541(2004)005<0487:CAMTPG>2.0.CO;2

Joyce, R. J., & Xie, P. (2011). Kalman filter–based CMORPH. *Journal of Hydrometeorology*, *12*(6), 1547–1563. https://doi.org/10.1175/JHM-D-11-022.1

Kaplan, J., & DeMaria, M. (2003). Large-scale characteristics of rapidly intensifying tropical cyclones in the North Atlantic basin. *Weather and Forecasting*, *18*(6), 1093–1108. https://doi.org/10.1175/1520-0434(2003)018<1093:LCORIT>2.0.CO;2

Kim, K., Park, J., Baik, J., & Choi, M. (2017). Evaluation of topographical and seasonal features using GPM IMERG and TRMM 3B42 over Far-East Asia. *Atmospheric Research*, *187*, 95–105. https://doi.org/10.1016/j.atmosres.2016.12.007

Knaff, J. A., Slocum, C. J., & Musgrave, K. D. (2019). Quantification and exploration of diurnal oscillations in tropical cyclones. *Monthly Weather Review*, *147*(6), 2105–2121. https://doi.org/10.1175/MWR-D-18-0379.1

Knapp, K. (2008). Calibration assessment of ISCCP geostationary infrared observations using HIRS. *Journal of Atmospheric and Oceanic Technology*, *25*(2), 183–195. https://doi.org/10.1175/2007JTECHA910.1

Knapp, K. R., & NOAA CDR Program. (2014). NOAA climate data record (CDR) of gridded satellite data from ISCCP B1 (GridSat-B1) infrared channel brightness temperature, version 2. [Dataset]. NOAA National Centers for Environmental Information. https://doi.org/10.7289/V59P2ZKR

Knapp, K. R., Ansari, S., Bain, C. L., Bourassa, M. A., Dickinson, M. J., Funk, C., et al. (2011). Globally gridded satellite observations for climate studies. *Bulletin of the American Meteorological Society*, *92*(7), 893–907. https://doi.org/10.1175/2011BAMS3039.1

Knapp, K. R., Diamond, H. J., Kossin, J. P., Kruk, M. C., & Schreck, C. J. (2018). International best track Archive for climate Stewardship (IBTrACS) Project, version 4. [Dataset]. NOAA National Centers for Environmental Information. https://doi.org/10.25921/82ty-9e16

Knapp, K. R., Kruk, M. C., Levinson, D. H., Diamond, H. J., & Neumann, C. J. (2010). The International best track Archive for climate Stewardship (IBTrACS): Unifying tropical cyclone data. *Bulletin of the American Meteorological Society*, *91*(3), 363–376. https://doi.org/10.1175/2009BAMS2755.1

Kossin, J. P. (2002). Daily hurricane variability inferred from GOES infrared imagery. *Monthly Weather Review*, *130*(9), 2260–2270. https://doi.org/10.1175/1520-0493(2002)130<2260:DHVIFG>2.0.CO;2

Kraus, E. B. (1963). The diurnal precipitation change over the sea. *Journal of the Atmospheric Sciences*, *20*(6), 551–556. https://doi.org/10.1175/1520-0469(1963)020<0551:TDPCOTDP>2.0.CO;2

Lee, J.-D., Wu, C.-C., & Ito, K. (2020). Diurnal variation of the convective area and eye size associated with the rapid intensification of tropical cyclones. *Monthly Weather Review*, *148*(10), 4061–4082. https://doi.org/10.1175/MWR-D-19-0345.1

Leppert, K. D., & Cecil, D. J. (2016). Tropical cyclone diurnal cycle as observed by TRMM. *Monthly Weather Review*, *144*(8), 2793–2808. https://doi.org/10.1175/MWR-D-15-0358.1

Leroux, M.-D., Wood, K., Elsberry, R., Cayanan, E., Hendricks, E., Kucas, M., et al. (2018). Recent advances in research and forecasting of tropical cyclone track, intensity, and structure at landfall. *Tropical Cyclone Research and Review*, *7*(2), 85–105.

Lin, S.-J., & Chou, K.-H. (2020). The Lightning distribution of tropical cyclones over the Western North Pacific. *Monthly Weather Review*, *148*(11), 4415–4434. https://doi.org/10.1175/MWR-D-19-0327.1

Ma, Q., Li, Y., Feng, H., Yu, Q., Zou, Y., Liu, F., & Pulatov, B. (2021). Performance evaluation and correction of precipitation data using the 20-year IMERG and TMPA precipitation products in diverse subregions of China. *Atmospheric Research*, *249*, 105304. https://doi.org/10.1016/j.atmosres.2020.105304

Mecikalski, J. R., & Tripoli, G. J. (1998). Inertial available kinetic energy and the dynamics of tropical plume formation. *Monthly Weather Review*, *126*(8), 2200–2216. https://doi.org/10.1175/1520-0493(1998)126<2200:IAKEAT>2.0.CO;2

Melhauser, C., & Zhang, F. (2014). Diurnal radiation cycle impact on the pregenesis environment of Hurricane Karl (2010). *Journal of the Atmospheric Sciences*, *71*(4), 1241–1259. https://doi.org/10.1175/JAS-D-13-0116.1

Mori, N., & Takemi, T. (2016). Impact assessment of coastal hazards due to future changes of tropical cyclones in the North Pacific Ocean. *Weather and Climate Extremes*, *11*, 53–69. https://doi.org/10.1016/j.wace.2015.09.002

Muramatsu, T. (1983). Diurnal variations of satellite-measured TBB areal distribution and eye diameter of mature typhoons. *Journal of the Meteorological Society of Japan Series II*, *61*(1), 77–90. https://doi.org/10.2151/jmsj1965.61.1_77

Navarro, E. L., & Hakim, G. J. (2016). Idealized numerical modeling of the diurnal cycle of tropical cyclones. *Journal of the Atmospheric Sciences*, *73*(10), 4189–4201. https://doi.org/10.1175/JAS-D-15-0349.1

Navarro, E. L., Hakim, G. J., & Willoughby, H. E. (2017). Balanced response of an Axisymmetric tropical cyclone to periodic diurnal heating. *Journal of the Atmospheric Sciences*, *74*(10), 3325–3337. https://doi.org/10.1175/JAS-D-16-0279.1

O'Neill, M., Perez-Betancourt, D., & Wing, A. (2017). Accessible environments for diurnal-period waves in simulated tropical cyclones. *Journal of the Atmospheric Sciences*, *74*(8), 2489–2502. https://doi.org/10.1175/JAS-D-16-0294.1

Randall, D. A., Harshvardhan, & Dazlich, D. A. (1991). Diurnal variability of the hydrologic cycle in a general circulation model. *Journal of the Atmospheric Sciences*, *48*(1), 40–62. https://doi.org/10.1175/1520-0469(1991)048<0040:DVOTHC>2.0.CO;2

Rodger, C. J., Brundell, J. B., Holzworth, R. H., Lay, E. H., Crosby, N. B., Huang, T. Y., & Rycroft, M. J. (2009). Growing detection efficiency of the World Wide lightning location Network. *AIP Conference Proceedings*, *1118*(1), 15–20. https://doi.org/10.1063/1.3137706

Rogers, R. F. (2021). Recent advances in our understanding of tropical Cyclone intensity change processes from airborne observations. *Atmosphere*, *12*(5), 650. https://doi.org/10.3390/atmos12050650

Rogers, R. F., Zhang, J. A., Zawislak, J., Jiang, H., Alvey, G. R., Zipser, E. J., & Stevenson, S. N. (2016). Observations of the structure and evolution of Hurricane Edouard (2014) during intensity change. Part II: Kinematic structure and the distribution of deep convection. *Monthly Weather Review*, *144*(9), 3355–3376. https://doi.org/10.1175/MWR-D-16-0017.1

Ruppert, J. H., & Hohenegger, C. (2018). Diurnal circulation adjustment and organized deep convection. *Journal of Climate*, *31*(12), 4899–4916. https://doi.org/10.1175/JCLI-D-17-0693.1

Ruppert Jr., J. H., & O'Neill, M. E. (2019). Diurnal cloud and circulation changes in simulated tropical cyclones. *Geophysical Research Letters*, *46*, 502–511. https://doi.org/10.1029/2018GL081302

Stevenson, S. N., Corbosiero, K. L., & Abarca, S. F. (2016). Lightning in eastern North Pacific tropical cyclones: A comparison to the North Atlantic. *Monthly Weather Review*, *144*(1), 225–239. https://doi.org/10.1175/MWR-D-15-0276.1

Stevenson, S. N., Corbosiero, K. L., DeMaria, M., & Vigh, J. L. (2018). A 10-year survey of tropical cyclone inner-core lightning bursts and their relationship to intensity change. *Weather and Forecasting*, *33*(1), 23–36. https://doi.org/10.1175/waf-d-17-0096.1

Stevenson, S. N., Corbosiero, K. L., & Molinari, J. (2014). The convective evolution and rapid intensification of Hurricane Earl (2010). *Monthly Weather Review*, *142*(11), 43644380–4380. https://doi.org/10.1175/MWR-D-14-00078.1

Sun, L., Tang, X., Zhuge, X., Tan, Z. M., & Fang, J. (2021). Diurnal variation of overshooting tops in typhoons detected by Himawari-8 Satellite. *Geophysical Research Letters*, *48*, e2021GL095565. https://doi.org/10.1029/2021GL095565

Susca-Lopata, G., Zawislak, J., Zipser, E. J., & Rogers, R. F. (2015). The role of observed environmental conditions and precipitation evolution in the rapid intensification of Hurricane Earl (2010). *Monthly Weather Review*, *143*(6), 2207–2223. https://doi.org/10.1175/MWR-D-14-00283.1

Tan, J., Huffman, G. J., Bolvin, D. T., & Nelkin, E. J. (2019). Diurnal cycle of IMERG V06 precipitation. *Geophysical Research Letters*, *46*, 13584–13592. https://doi.org/10.1029/2019GL085395

Tang, X., Tan, Z.-M., Fang, J., Munsell, E. B., & Zhang, F. (2019). Impact of the diurnal radiation contrast on the contraction of radius of maximum wind during intensification of Hurricane Edouard (2014). *Journal of the Atmospheric Sciences*, *76*(2), 421–432. https://doi.org/10.1175/JAS-D-18-0131.1

Tang, X., & Zhang, F. (2016). Impacts of the diurnal radiation cycle on the formation, intensity, and structure of Hurricane Edouard (2014). *Journal of the Atmospheric Sciences*, *73*(7), 2871–2892. https://doi.org/10.1175/JAS-D-15-0283.1

Trabing, B. C., & Bell, M. M. (2021). Observations of diurnal variability under the cirrus canopy of Typhoon Kong-rey (2018). *Monthly Weather Review*, *149*(9), 2954–2964. https://doi.org/10.1175/MWR-D-20-0327.1

Vigh, J., & Schubert, W. (2009). Rapid development of tropical cyclone warm core. *Journal of The Atmospheric Sciences*, *66*(11), 3335–3350. https://doi.org/10.1175/2009JAS3092.1

Virts, K. S., Wallace, J. M., Hutchins, M. L., & Holzworth, R. H. (2013). Highlights of a new ground-based, hourly global lightning climatology. *Bulletin of the American Meteorological Society*, *94*(9), 1381–1391. https://doi.org/10.1175/BAMS-D-12-00082.1

Wu, Q., & Hong, J. (2022). Diurnal variations in contraction of the radius of maximum tangential wind in tropical cyclones. *Geophysical Research Letters*, *49*(3). https://doi.org/10.1029/2021gl096048

Wang, Y., & Wu, C. C. (2004). Current understanding of tropical cyclone structure and intensity changes: A review. *Meteorology and Atmospheric Physics*, *87*(4), 257–278. https://doi.org/10.1007/s00703-003-0055-6

Wang, Z. (2014). Role of cumulus congestus in tropical cyclone formation in a high-resolution numerical model simulation. *Journal of the Atmospheric Sciences*, *71*(5), 1681–1700. https://doi.org/10.1175/JAS-D-13-0257.1

Wang, Z. (2018). What is the key feature of convection leading up to tropical cyclone formation? *Journal of the Atmospheric Sciences*, *75*(5), 1609–1629. https://doi.org/10.1175/JAS-D-17-0131.1

Weinkle, J., Maue, R., & Pielke, R. (2012). Historical global tropical cyclone landfalls. *Journal of Climate*, *25*(13), 4729–4735. https://doi.org/10.1175/JCLI-D-11-00719.1

Wu, Q., Hong, J., & Ruan, Z. (2020). Diurnal variations in tropical cyclone intensification. *Geophysical Research Letters*, *47*, e2020GL090397. https://doi.org/10.1029/2020GL090397

Wu, Q., & Ruan, Z. (2016). Diurnal variations of the areas and temperatures in tropical cyclone clouds. *Quarterly Journal of the Royal Meteorological Society*, *142*(700), 2788–2796. https://doi.org/10.1002/qj.2868

Zhang, J. A., Dunion, J. P., & Nolan, D. S. (2020). In situ observations of the diurnal variation in the boundary layer of mature hurricanes. *Geophysical Research Letters*, *47*, e2019GL086206. https://doi.org/10.1029/2019GL086206

Zhang, Q., Gu, X., Shi, P., & Singh, V. P. (2017). Impact of tropical cyclones on flood risk in southeastern China: Spatial patterns, causes and implications. *Global and Planetary Change*, *150*, 81–93. https://doi.org/10.1016/j.gloplacha.2017.02.004

Zhang, Q., Wu, L., & Liu, Q. (2009). Tropical cyclone damages in China 1983–2006. *Bulletin of the American Meteorological Society*, *90*(4), 489–496. https://doi.org/10.1175/2008BAMS2631.1

Zhang, X., & Xu, W. (2021a). Diurnal variations in rainfall and precipitation asymmetry of tropical cyclones in the Northwest Pacific Region. *Journal of Climate*, 5565–5582. https://doi.org/10.1175/JCLI-D-20-0795.1

Zhang, X., & Xu, W. (2021b). Strong diurnal pulsing of cold clouds in rapidly intensifying tropical cyclones. *Geophysical Research Letters*, *48*, e2021GL094773. https://doi.org/10.1029/2021GL094773

Zhang, X., & Xu, W. (2022). Is there an outward propagating diurnal signal in the precipitation of tropical cyclones? *Geophysical Research Letters*, *49*, e2021GL097166. https://doi.org/10.1029/2021GL097166